JOURNAL OF GEOPHYSICAL RESEARCH, VOL. 113, C07032, doi:10.1029/2007JC004598, 2008

How does ocean biology affect atmospheric pCO_2? Theory and models

I. Marinov,[1,2] M. Follows,[2] A. Gnanadesikan,[3] J. L. Sarmiento,[4] and R. D. Slater[4]

Received 18 October 2007; revised 26 February 2008; accepted 21 March 2008; published 22 July 2008.

[1] This paper examines the sensitivity of atmospheric pCO_2 to changes in ocean biology that result in drawdown of nutrients at the ocean surface. We show that the global inventory of preformed nutrients is the key determinant of atmospheric pCO_2 and the oceanic carbon storage due to the soft-tissue pump (OCS_{soft}). We develop a new theory showing that under conditions of perfect equilibrium between atmosphere and ocean, atmospheric pCO_2 can be written as a sum of exponential functions of OCS_{soft}. The theory also demonstrates how the sensitivity of atmospheric pCO_2 to changes in the soft-tissue pump depends on the preformed nutrient inventory and on surface buffer chemistry. We validate our theory against simulations of nutrient depletion in a suite of realistic general circulation models (GCMs). The decrease in atmospheric pCO_2 following surface nutrient depletion depends on the oceanic circulation in the models. Increasing deep ocean ventilation by increasing vertical mixing or Southern Ocean winds increases the atmospheric pCO_2 sensitivity to surface nutrient forcing. Conversely, stratifying the Southern Ocean decreases the atmospheric CO_2 sensitivity to surface nutrient depletion. Surface CO_2 disequilibrium due to the slow gas exchange with the atmosphere acts to make atmospheric pCO_2 more sensitive to nutrient depletion in high-ventilation models and less sensitive to nutrient depletion in low-ventilation models. Our findings have potentially important implications for both past and future climates.

Citation: Marinov, I., M. Follows, A. Gnanadesikan, J. L. Sarmiento, and R. D. Slater (2008), How does ocean biology affect atmospheric pCO_2? Theory and models, *J. Geophys. Res.*, *113*, C07032, doi:10.1029/2007JC004598.

1. Introduction

[2] The objective of this study is to understand how atmospheric pCO_2 (pCO_{2a}) is related to oceanic biological cycling and circulation. This question is relevant to one of the most heated debates of the past two decades in oceanography, the attempt to understand the large decreases (of order 80 ppm) in CO_2 that occurred in going from interglacial to glacial periods as observed in ice-core records [*Petit et al.*, 1999]. In a series of box model studies, *Sarmiento and Toggweiler* [1984], *Knox and McElroy* [1984], and *Siegenthaler and Wenk* [1984] proposed that increased drawdown of high-latitude nutrients and CO_2 associated with a stronger biological pump was responsible for the lower atmospheric CO_2 during ice ages. This line of reasoning connects glacial-interglacial variation in pCO_{2a} to the existence of HNLC (high nutrient, low chlorophyll) areas in the world ocean. These regions (Equatorial Pacific, Subpolar Pacific and the Southern Ocean) continue to puzzle ocean biogeochemists because of the presence of large quantities of unused nutrients, which would be expected to fuel high biological production, in an otherwise low productivity (low chlorophyll) region.

[3] On the basis of bottle experiments, John H. Martin postulated that large-scale addition of iron (Fe) to the HNLC regions would lead to enhanced biological productivity and reduced atmospheric CO_2 [*Martin*, 1990]. Martin's hypothesis that an increase of iron in windblown continental dust could trigger Ice Ages inspired experimental work and Fe enrichment experiments such as IronEx I and II, SOIREE, SOFeX, Eisenex [e.g., *Buesseler et al.*, 2004; *Boyd et al.*, 2007, and references therein], as well as box model and GCM studies [e.g., *Sarmiento and Orr*, 1991; *Archer et al.*, 2000; *Matear and Elliott*, 2004; *Dutkiewicz et al.*, 2005]. The artificial increase of biological production via iron fertilization has been proposed as a potential mechanism to offset present and future anthropogenic greenhouse emissions.

[4] Subsequent work has shown that the effectiveness of this mechanism may depend on ocean circulation [*Archer et al.*, 2000; *Broecker et al.*, 1999; *Bacastow*, 1996]. Archer et al. showed that various GCMs have different sensitivities to high-latitude forcing as measured by their abiotic pCO_2, i.e., the atmospheric pCO_2 resulting from running the abiotic model without the biological pump included. Broecker et al. designed an index, HBEI, which reflects the extent to which

[1]Department of Marine Chemistry and Geochemistry, Woods Hole Oceanographic Institution, Woods Hole, Massachusetts, USA.
[2]Program in Atmospheres, Oceans, and Climate, Massachusetts Institute of Technology, Cambridge, Massachusetts, USA.
[3]Geophysical Fluid Dynamics Laboratory, NOAA, Princeton, New Jersey, USA.
[4]Atmospheric and Oceanic Sciences Program, Princeton University, Princeton, New Jersey, USA.

0148-0227/08/2007JC004598$09.00

atmospheric pCO_2 is determined by the cold high-latitude waters versus the warm low-latitude surface waters. The HBEI index was shown to vary considerably between different GCMs and between box models and GCMs. The HBEI index and the abiotic pCO_2 of Archer measure the sensitivity of the system to changes in the solubility pump, while turning off or keeping the biological pump constant.

[5] Here we present an alternative biological approach to these solubility pump-focused studies, indirectly estimating the potential impact of Fe fertilization on the global carbon cycle by forcing surface nutrients to zero in a large ocean area for a few thousand years. As such, our simulations likely provide an upper limit estimate of the ocean uptake under long-term Fe fertilization. Our purpose is to analyze what determines the sensitivity of atmospheric pCO_2 to surface nutrient depletion, and how this sensitivity depends on sub-grid-scale mixing, wind intensity and gas exchange. Section 2 introduces the model suite, explains major circulation differences between our models and details the simulations performed. Section 3.1 compares the outcome of nutrient depletion in the Southern Ocean, North Atlantic, North Pacific and the tropics. Section 3.2 compares the relative roles of the soft-tissue, carbonate or solubility pumps in reducing atmospheric pCO_2 following nutrient depletion. This leads to the central results of our paper (sections 3.3–3.5).

[6] In section 3.3 we propose a new theory, along the lines of *Ito and Follows* [2005] and *Marinov et al.* [2008] on how atmospheric pCO_2 changes with preformed phosphate and the ocean carbon storage due to the soft-tissue pump. We test our theory in models and systematically address the following questions: (1) What is the role of ocean circulation and mixing in setting the high-latitude sensitivity of pCO_{2a} to changes in surface nutrients? (2) How will gas exchange affect the response of atmospheric pCO_2 to nutrient depletion?

[7] To answer the first question, we analyze in section 3.4 results of surface nutrient depletion simulations in an extended suite of models with different isopycnal mixing, diapycnal mixing and Southern Ocean winds.

[8] Gas exchange obscures the biological signal; it is therefore important to separate the effects of gas exchange from those solely due to biology. To answer the second question, depletion simulations are run in model setups in which the CO_2 exchange at the ocean surface is either realistically slow (allowing for some surface CO_2 disequilibrium) or infinitely fast. Section 3.5 shows that the extent of surface CO_2 disequilibrium in the slow gas exchange models depends on oceanic circulation, and can strongly influence the outcome of nutrient depletion experiments.

2. Model Description, Simulations Performed, and Basic Ocean Circulation

[9] Our study uses the Geophysical Fluid Dynamics Laboratory Modular Ocean Model (MOM) version 3 [*Pacanowski and Griffies*, 1999], a well-studied model which we have used for previous biogeochemistry work [e.g., *Gnanadesikan et al.*, 2002, 2003, 2004; *Marinov et al.*, 2006, 2008]. The biogeochemical component of the model is consistent with OCMIP-2 (Ocean Carbon Modeling Initiative Project) specifications [e.g., *Najjar et al.*, 2007] (also R. J. Najjar and J. Orr, Design of OCMIP-2 simulations of chlorofluorocarbons, the solubility pump and common biogeochemistry, 1999, available at http://www.ipsl.jussieu.fr/OCMIP). A single well-mixed atmospheric box is coupled to the ocean carbon cycle. The model simulates production and remineralization of both dissolved and particulate organic matter. Standard prognostic variables calculated at each time step are phosphate (PO_4^{3-}), oxygen (O_2), dissolved organic phosphate (DOP), dissolved inorganic carbon (DIC) and alkalinity (ALK). Global mean values are chosen for initial conditions: DIC = 2230 μmol/kg, ALK = 2370 μmol/kg. Model currency is PO_4^{3-}.

[10] New production is obtained by restoring surface PO_4^{3-} to a value PO_4^* in the upper 75 m of the model:

$$\begin{aligned} Jprod(x,y,z,t) &= \left(PO_4^{3-}(x,y,z,t) - PO_4^*(x,y,z,t)\right)/\tau \\ &\qquad \text{for } PO_4^{3-} > PO_4^*, \\ Jprod(x,y,z,t) &= 0 \qquad \text{for } PO_4 \le PO_4^*, \end{aligned} \tag{1}$$

where the biological timescale is τ = 30 days.

[11] For each model considered in this paper we run a control simulation and a depletion simulation. In all control simulations nutrients are restored to the observed seasonally varying concentrations of *Louanchi and Najjar* [2000], i.e., $PO_4^* = PO_4^{obs}$ in the above equation. In the depletion simulations, PO_4^* is set to zero in a given ocean area. For example, in the Southern Ocean nutrient depletion scenarios, nutrients are restored to $PO_4^* = 0$ south of 30°S and to $PO_4^* = PO_4^{obs}$ everywhere else.

[12] Two thirds of the production goes to DOP, which is consumed everywhere following first-order kinetics with a remineralization timescale of 6 months, The remainder results in an instantaneous flux of particulate organic phosphorus at the compensation depth. This flux decreases with depth below 75 m owing to remineralization following a power law function. P-based fluxes such as export production are converted to carbon units via a stoichiometric ratio $r_{C:P}$ of 117. For further description of the basic biogeochemical model see *Gnanadesikan et al.* [2002] and *Najjar et al.* [2007].

[13] We also introduce preformed PO_4^{3-} as a prognostic variable as in work by *Marinov et al.* [2006]. Preformed PO_4^{3-} is set equal to PO_4^{3-} at the ocean surface and is a biologically conserved tracer everywhere in the ocean interior. Total amount of PO_4 in the ocean is kept constant and equal between all models studied here. Finally, we note that while not state of the art, the present model is perfectly suited for the present investigation.

2.1. Nine Model Setups With Different Circulation

[14] Our GCM uses the Gent-McWilliams [*Gent and McWilliams*, 1990] parameterization of sub-grid-scale processes, with tracer mixing represented by the diapycnal (cross-isopycnal) mixing coefficient K_v and by the isopycnal mixing coefficient A_i.

[15] Nine different versions of MOM3 are designed as summarized in Table 1. Five of these model setups are based on work by *Gnanadesikan et al.* [2002, 2003, 2004] and use seasonal wind stresses of *Hellerman and Rosenstein* [1983] (HR) as upper boundary condition for the momen-

Table 1. Model Design[a]

Model	K_v	A_i	Wind Forcing
	Lower Ventilation Models		
LL (standard)	hyperbolic variation from 0.15 cm^2/s at surface to 1.3 cm^2/s at 5000 m	1000 m^2/s	HR
high A_i	idem LL	2000 m^2/s	HR
windx0.5	idem LL	idem LL	HR decreased by 50% in S. Ocean
high South K_v	idem LL south of 45°S, 1.3 cm^2/s at all depths south of 55°S, linearly interpolated between 45°S–55°S	idem LL	HR
	Higher-Ventilation Models		
high K_v	hyperbolic variation from 0.6 cm^2/s at surface to 1.3 cm^2/s at 5000 m	idem LL	HR
high A_i-high K_v	idem HL	2000 m^2/s	HR
P2A	as in high south K_v with some modifications (see text)	idem LL	see text
windx2	idem LL	idem LL	HR increased twofold in Southern Ocean
windx3	idem LL	idem LL	HR increased threefold in Southern Ocean

[a]Our nine models have different diapycnal mixing (K_v), isopycnal mixing (A_i) and wind forcing. HR are seasonal winds stresses of *Hellerman and Rosenstein* [1983]. Models can be roughly separated into low- and high-ventilation categories, depending on the net ventilation of the deep waters via the Southern Ocean (see section 2.2 and Figure 1).

tum equation. These are LL, high K_v, high South K_v, high A_i, high A_i-high K_v.

[16] LL stands for the low A_i and low K_v model case. In our standard or LL model, diapycnal mixing K_v varies hyperbolically in the ocean from 0.15 cm^2/s at the surface to 1.3 cm^2/s at 5000 m with a hyperbolic tangent transition at 2500 m [*Bryan and Lewis*, 1979], while isopycnal mixing A_i is set to 1000 m^2/s everywhere in the ocean.

[17] Relative to our standard model, we can increase either K_v alone (as in models high K_v or high South K_v), A_i alone (model high A_i), or we increase both K_v and A_i (high A_i-high K_v model).

[18] The P2A model is the Princeton model with the most realistic distributions of tracers (radiocarbon, global particle export, AOU) when compared to measurements [*Gnanadesikan et al.*, 2004]. In the P2A model K_v has the same structure as in the high South K_v model except for higher vertical mixing between the top two boxes (50 cm^2/s). Additionally, this model uses ECMWF wind stress forcing (about 1.5 times stronger than the regular HR wind stresses in the Southern Ocean), a Drake Passage narrowed by one grid box, and different heat and salt flux forcing fields. The nomenclature P2A (Princeton model version 2A) was kept for consistency with previous work [*Gnanadesikan et al.*, 2004].

[19] To explore the effect of extreme Southern Ocean wind stress we design three other models where winds are set to HR everywhere except south of 30°S where wind stress is either increased three fold (windx3 model), increased two fold (windx2 model) or decreased by 50% (windx0.5 model) relative to the LL model (Figure 1i).

2.2. Basic Ocean Circulation

[20] One can divide the flows ventilating the deep ocean into two basic circulations which pass through the Southern Ocean. Ekman divergence driven by wind forces deep water rich in nutrients and DIC to upwell in an area south of the Antarctic Polar Front. Once at the surface, a fraction of this water moves northward and eventually gets subducted either as Antarctic Intermediate Water (AAIW) or as Subantarctic Mode Water (SAMW), penetrates northward to the rest of the ocean at intermediate depths and returns to the Southern Ocean via the North Atlantic Deep Water (NADW). This is the upper circulation. Another fraction moves southward and is subducted as Antarctic Bottom Water (AABW); this is the lower circulation. We note that the lower and upper circulations reflect the residual mean circulation, which accounts for both Ekman forcing and the integral effect of eddy transfers.

[21] Figure 1 shows the meridional overturning circulation and convective indices in three of our models. A stronger diapycnal mixing K_v or stronger Southern Ocean westerlies result in increased Southern Ocean upwelling, increased AABW formation and increased Southern Ocean deep convection. This is confirmed by $\Delta^{14}C$ values (Figures 1g and 1h), which indicate younger deep waters and more vigorous deep water ventilation in the high K_v, windx2, and windx3 models compared to the LL model. Conversely, weaker westerlies or increased isopycnal mixing A_i result in weaker AABW formation and weaker convection, as indicated by lower $\Delta^{14}C$ values in the windx0.5 and high A_i models compared to the LL model.

[22] For simplicity we refer here to the LL, high A_i and windx0.5 models as our low-ventilation models and to high K_v, P2A, windx2, windx3 as the high-ventilation models. *Marinov et al.* [2008] discussed the connection between globally averaged preformed PO_4^{3-} and the strength of deep water ventilation, demonstrating that high-ventilation models tend to have higher preformed PO_4^{3-} and low-ventilation models tend to have lower preformed PO_4^{3-} independent of changes in surface nutrients (Figures 1g and 1h). Here we discuss how these ventilation differences impact the drawdown in atmospheric pCO_2 following surface nutrient depletion.

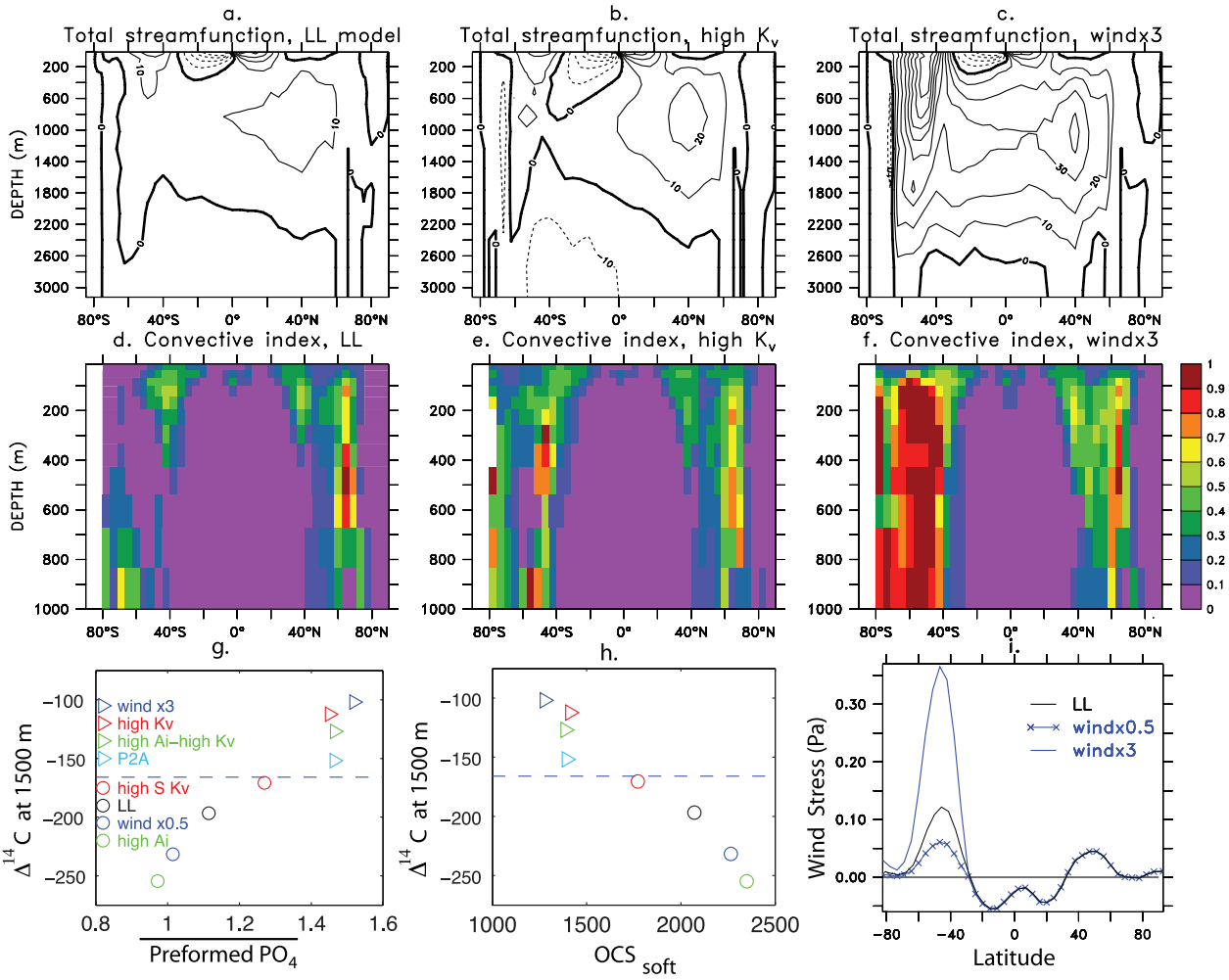

Figure 1. (a–c) Overturning stream function in Sv calculated as the zonal and depth integral of the meridional velocity for the LL (control), high K_v, high Southern Ocean wind models. Shown stream functions are the sum between the GM and Euler stream functions. (d–f) Zonally averaged convective indices for the three models. Convective index is 1 when convection is on. A value of 0.5 can mean that half of the points at a given location are convecting all the time,that all points convect half of the time, or a scenario in between these two. (g and h) Covariation of Δ^{14}C (globally averaged at 1500 m) with globally averaged Preformed PO_4 (μmol/kg) and OCS_{soft} in the control simulations. The ocean carbon storage due to the soft-tissue pump (PgC) is calculated as $OCS_{soft} = V_{oc} \cdot r_{C:P} \cdot (\overline{PO_4} - \overline{PO_{4pref}})$. Deep waters in the high K_v and windx3 models are the youngest, best ventilated water masses while deep waters in the high A_i and windx0.5 models are oldest, least ventilated. Annual mean results shown in all cases. The horizontal lines show the observed Δ^{14}C at 1500 m from GLODAP. (i) Annually and zonally averaged wind stresses for three of the models. Westerlies are positive.

2.3. Running Our Models

2.3.1. Separating the Carbon Pumps

[23] The partition of CO_2 between the atmosphere and the ocean is determined by a combination of physical, chemical and biological processes collectively known as the ocean carbon pump. A strong carbon pump signals a large storage of inorganic carbon in the deep ocean relative to the surface. The ocean carbon pump is the sum of the abiotic or solubility pump (a function of temperature and salinity since these affect the surface air-sea CO_2 exchange), the soft-tissue pump (a function of photosynthesis and remineralization), and the carbonate pump (a function of $CaCO_3$ formation and dissolution). In order to separate these pumps from each other we consider three different scenarios: a full carbon pump scenario, in which all of the carbon pumps are turned on; a biology pump only scenario, in which only the soft-tissue and carbonate pumps are turned on; and a soft-tissue pump scenario, in which only the soft-tissue pump is turned on. Appendix A details this pump separation.

2.3.2. Simulation Design for Sections 3.1 and 3.2 (Table 2)

[24] The nine circulation models described in Table 1 are run separately to equilibrium from an arbitrary DIC distri-

Table 2. General Circulation Models and Corresponding Nutrient Depletion Simulations Performed[a]

Carbon Pump Scenarios Gas Exchange Setup	Nutrient Depletion Area	Circulation Model Used
Full carbon pump RGE	Southern Ocean (90°S–30°S)	LL, high A_i,high K_v
	North Atlantic (30°S–80°N)	high K_v, high A_i-highK_v
	North Pacific (30°N–67°N)	
	tropics (18°S–18°N)	
Biology pump only RGE	Southern Ocean (90°S–30°S)	LL and high K_v
Soft-tissue pump RGE and FGE	Southern Ocean (90°S–30°S)	all circulation models

[a]RGE and FGE correspond to regular and fast gas exchange simulations. Model design detailed in section 2.3 and Appendix A.

bution with a fixed preindustrial atmosphere of 278 ppm by allowing CO_2 to invade the ocean until the absolute value of the global, annual mean air-sea CO_2 flux is less than 0.01 PgC/a. For each of the circulation models, the resulting state is used to initialize both control and depletion simulations.

[25] In the control simulations, each model is further run to equilibrium while keeping the total amount of inorganic carbon in the ocean-atmosphere system constant (allowing atmospheric CO_2 to vary) and without any changes to the system. In the depletion simulations, each model is run to a new equilibrium state while continuously restoring surface nutrients to zero in a given region of the ocean as explained earlier in this section. The total inorganic carbon in the system is again kept constant, while atmospheric CO_2 is allowed to vary. The response of all chemical species (including atmospheric pCO_2) to nutrient depletion is calculated in each case relative to the control simulation ran for the same number of years. We note that in all our simulations models with intensified overall circulation and deep ocean ventilation (high K_v, P2A, high A_i-highK_v, windx3) reach equilibrium much faster than models with slow circulation (LL, high A_i, windx0.5).

[26] The relative fractions of inorganic carbon in the ocean and atmosphere pools are different in different circulation models. Therefore, by imposing a fixed atmospheric pCO_2 of 278 ppm at the beginning of our control and depletion simulations, we are basically allowing each of the circulation models to have a different total carbon in the ocean-atmosphere system. This simulation setup agrees with the original OCMIP protocol [*Najjar et al.*, 2007].

[27] For a given physical model we run the control and Southern Ocean depletion simulations in each of three scenarios: the full carbon pump, biological pump only and soft-tissue pump only. Simulations performed for sections 3.1 and 3.2 are summarized in Table 2. Section 3.1 analyzes the response of atmospheric pCO_2 to four different large scale nutrient depletions in models run with a full carbon pump. Section 3.2 analyzes the response of the different carbon pumps to depletion.

2.3.3. Simulation Design for Sections 3.3–3.5: Soft-Tissue Pump Models (Table 3)

[28] In sections 3.3–3.5 we analyze the outcome of Southern Ocean nutrient depletion simulations in the soft-tissue-only versions of our nine circulation models. Model properties and simulations used in this part of the paper are summarized in Table 3. We note one very important difference from the simulations performed for sections 3.1 and 3.2. We now require that the total amount of inorganic carbon in the air-ocean system is constant at all times and identical across all models; that is, we assume a closed system with respect to inorganic carbon. Allowing the total carbon burden to vary would introduce small variations from the theory developed in section 3.3; such effects will need to be analyzed in depth at a later time.

[29] After bringing the LL model to equilibrium we calculate the total amount of inorganic carbon in the system (total ocean DIC plus total atmospheric CO_2). For each of the nine (soft-tissue-only) circulation models we then run both control and nutrient depletion simulations while keeping the total amount of inorganic carbon in the ocean-air system constant and identical with the one calculated for the LL model above. While the partitioning of inorganic carbon between the ocean and atmosphere pools is different in different circulation models and changes with nutrient depletion, this procedure ensures that the total carbon in the ocean-atmosphere system is identical across all models.

[30] The degree to which CO_2 at the ocean surface equilibrates with the atmosphere impacts the net carbon storage in the deep ocean and therefore the outcome of nutrient depletion experiments. In order to understand this impact we perform all nutrient depletion experiments in both models with fast gas exchange (FGE) and regular gas exchange (RGE).

[31] We simulate fast gas exchange by restoring DIC in the top layer of the model to the equilibrium DIC calculated from T and S at each time step and in each ocean surface grid cell and atmospheric pCO_2 at that time step. The timescale for restoring of surface DIC, given by the model time step, represents a fundamental limit on the CO_2 gas exchange. Thus, while CO_2 exchange in the FGE scenarios is not infinitely fast, it is the fastest gas exchange that can be achieved in a model. In our realistic RGE scenarios, CO_2 is out of equilibrium with the atmosphere; the amount of surface disequilibrium depends on the model circulation chosen. Section 3.4 focuses on the FGE models. Section 3.5 compares FGE and RGE simulations to understand the

Table 3. Model Characteristics and Simulations Performed for Sections 3.3–3.5

	Model Characteristics and Soft-Tissue Pump Simulations
Nine basic models	LL (standard), high south K_v, high K_v, high A_i, high K_v-high A_i, windx0.5, windx2, windx3, P2A
Scenarios	soft-tissue pump scenarios
Gas exchange	all simulations performed for both FGE and RGE
Additional model characteristics	no ice, preformed PO_4 tracer included total inorganic carbon in air-ocean system and ocean PO_4 inventory identical in all models and for all simulations
Simulations performed	control simulations and Southern Ocean nutrient depletion for all nine models; global nutrient depletion for subset of seven models

Table 4. Drawdown in Atmospheric pCO_2 Following Continuous Large-Scale Nutrient Depletion in Each of Four Ocean Areas[a]

	Depletion Scenario					
	LL	High A_i	High South K_v	High K_v	High A_i–High K_v	Sarm/Orr
Southern Ocean (90°S–30°S)	47.2 (63.5)	44.7	55.2	64.7	68.6 (78.8)	71.8
Tropics (18°S–18°N)	5.0 (4.4)	4.7	4.8	4.0	3.6 (3.2)	2.8
North Atlantic (30°S–80°N)	11.8 (15.0)	12.2	11.1	9.6	10.2(11.8)	12.7
North Pacific (30°N–67°N)	4.1 (3.7)	4.0	3.8	4.7	4.5(3.9)	6.9
Total change in pCO_{2atm}	68.1 (86.6)	65.6	74.9	83.0	86.9 (97.7)	94.4

[a]Given in ppm. Results shown after 500 years of continuous depletion in models with regular gas exchange and full carbon pump. For each depletion simulation atmospheric pCO_2 decrease is calculated relative to a control simulation run for the same number of years. In parentheses we show results after 2500 years for the Southern Ocean depletion scenarios, and after 1000 years for all other depletion scenarios for two of our models. All high A_i–highK_v values in parentheses and the LL Southern Ocean depletion value in parentheses are at equilibrium. Last column shows results from *Sarmiento and Orr* [1991] after 100 years of model run for comparison.

response of surface CO_2 disequilibrium to surface nutrient depletion.

3. Results

3.1. Nutrient Depletion Most Effective in the Southern Ocean

[32] In order to understand what areas of the ocean respond most to nutrient depletion we restore surface nutrients to zero in the Southern Ocean south of 30°S, the North Atlantic (30°N–80°N), the North Pacific (30°N–67°N), and the tropical band (18°S–18°N) as described in section 2.3. The resulting atmospheric pCO_2 drawdown after 500 years or more of continuous nutrient depletion in five different models is compared to previous results of *Sarmiento and Orr* [1991] (Table 4).

[33] Forcing nutrients to zero in a large ocean area increases biological export production locally, decreases surface CO_2 and forces additional CO_2 from the atmosphere into the ocean. If the increase in biological production occurs continuously for hundreds to thousands of years, the resulting drawdown in atmospheric pCO_2 is significant.

[34] Nutrient depletion is most efficient in regions where there is a direct communication between the surface and deep ocean via advective or convective pathways and where surface nutrients are highest, such as the Southern Ocean and the North Atlantic (Table 4). In these regions the additional CO_2 penetrates to the deep ocean where it is virtually trapped and is less likely to escape to the atmosphere. Because the Southern Ocean is the region where half of the ocean's deep waters are formed and unutilized surface nutrients are highest, this region is most effective at drawing down atmospheric pCO_2.

[35] Since there are no Pacific mechanisms of deep water formation equivalent to the AABW or NADW, the additional uptake of CO_2 in the North Pacific following nutrient depletion in this region does not penetrate far into the water column. Instead, it is transported southward at intermediate depths and released back to the atmosphere primarily in the Pacific subtropics north of the Equator.

[36] Results are similar in magnitude to those of *Sarmiento and Orr* [1991]. For all high-latitude regional depletions the atmospheric pCO_2 drawdown is smaller in our standard low-diffusion LL model compared to the Sarmiento and Orr model, likely because our model (unlike theirs) uses the Gent-McWilliams parameterization of subgrid-scale mixing and therefore has weaker and more realistic convective mixing in the Southern Ocean. The Sarmiento and Orr model is therefore more similar to our high K_v and high A_i-highK_v models which have stronger Southern Ocean convection (Figure 1).

3.2. Soft-Tissue Pump More Important Than the Carbonate and Solubility Pumps in the Nutrient Depletion Process

[37] In order to quantify the role of soft-tissue, carbonate and solubility pumps on atmospheric pCO_2 drawdown we perform Southern Ocean depletion simulations in the soft-tissue pump, biology pump only and full carbon pump scenarios as described in detail in Appendix A. In each simulation nutrients are continuously depleted at the ocean surface for a few thousand years until a new equilibrium is achieved.

[38] Table 5 and Figure 2 demonstrate that the atmospheric pCO_2 response to depletion is primarily driven by the soft-tissue pump. Table 5 shows that atmospheric pCO_2 drawdown is very similar when nutrient depletion is performed in models which include only the soft-tissue pump, only the biological pump (soft tissue+carbonate) or the full carbon pump (soft tissue+carbonate+solubility).

[39] For each of the soft-tissue, biological and full carbon pump scenarios the surface-to-deep DIC difference can be interpreted as a measure of the respective pump strength [*Volk and Hoffert*, 1985]. The solubility pump is the difference between the full carbon pump and the biological pump, while the carbonate pump is the difference between the biological and soft-tissue pumps [*Marinov and Sarmiento*, 2004]. Figure 2 shows that the changes in the

Table 5. Decrease in Atmospheric pCO_2 Following Nutrient Depletion South of 30°S in the LL and High K_v Soft-Tissue Models With and Without Ice, Biological Models With and Without Ice, and Full Model With Ice at Equilibrium[a]

	Model Type		
	Soft (Soft No Ice)	Bio (Bio No Ice)	Full Model
LL	70.1 (73.3)	74.3 (82.9)	63.5
High K_v	76.0 (73.2)	78.6 (75.7)	74.0

[a]The full model accounts for geographically variable surface T and S while the soft and biological models keep surface T and S equal to 10°C and 34.7 psu, respectively, in the gas exchange calculation. Soft-tissue model is identical with the biological model except for constant ALK, and thus no $CaCO_3$ formation or dissolution.

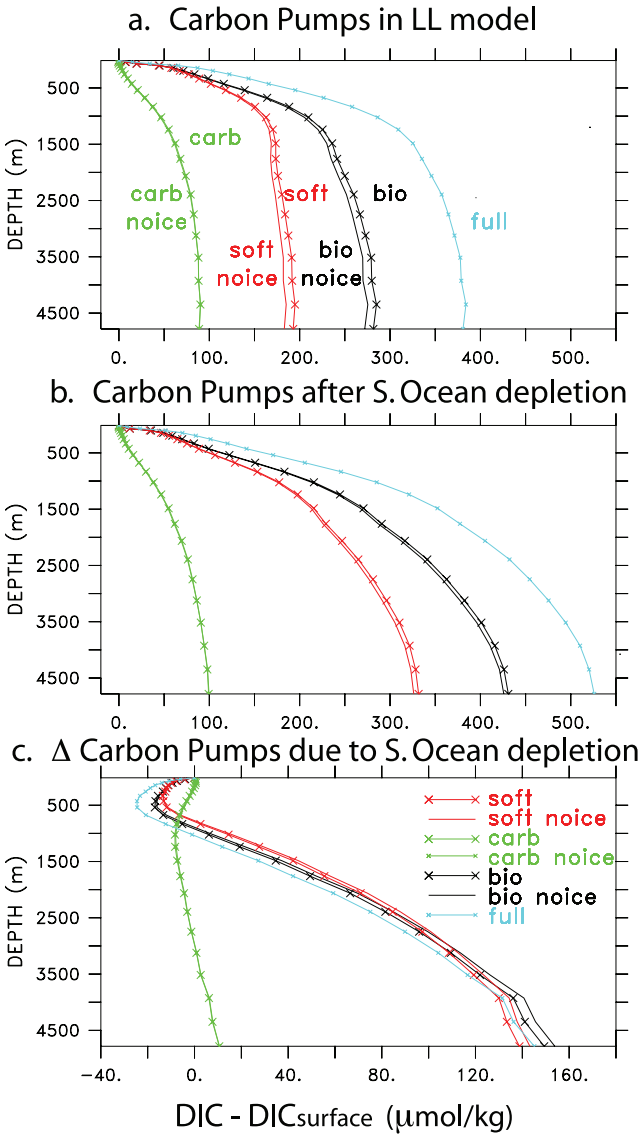

Figure 2. Globally averaged DIC at a given depth minus the average surface DIC, a measure of the carbon pumps, shown (a) in the control simulations and (b) after Southern Ocean nutrient depletion. (c) Change in the soft-tissue, carbonate, biological (soft tissue+carbonate), and full (soft+carbonate+solubility) carbon pumps due to depletion. Results shown at equilibrium for our standard LL models. Units are μmol/kg. Nutrient depletion affects primarily the soft-tissue pump, and has little impact on the carbonate pump (Figure 2c). The presence of ice has a minimal impact on the results. Separation of the pumps detailed in Appendix A and section 2.3.

surface-to-deep DIC gradients due to Southern Ocean depletion are almost identical in the soft-tissue, biological pump and full pump scenarios. Changes in the soft-tissue pump therefore account for the vast majority of the observed atmospheric carbon dioxide decrease in the full model which includes the soft-tissue, carbonate and solubility pumps.

[40] While $CaCO_3$ contributes about 100 μmol/kg or a third of the total surface to deep DIC gradient in the undepleted biological models (Figure 2a), it plays a modest role in the oceanic uptake of CO_2 following surface nutrient depletion. Figure 2c shows that a modest percent of the change in surface-to-deep DIC gradient when all carbon pumps are present is due to changes in the carbonate pump. The carbonate pump acts to increase CO_2 uptake by 2.6 ppm in the high K_v and by 4.2 ppm in the LL biological models relative to the corresponding soft-tissue models (compare entries for the biological and soft-tissue models in Table 5). Increased Southern Ocean biological production results in more local calcium carbonate formation. Each 1 mol increase in $CaCO_3$ results in a 2 mol decrease in ALK and a 1 mol decrease in DIC. A decrease in DIC results in a decrease in ocean pCO_2 while a decrease in ALK results in an increase in the carbon holding capacity of the ocean and thus in higher oceanic pCO_2. The low rain ratio (defined as the ratio of $CaCO_3$ flux to export flux of organic matter) in the OCMIP protocol ensures however that changes in $CaCO_3$ formation at the ocean surface have a minimal impact on oceanic pCO_2 and the net uptake of atmospheric CO_2.

[41] The solubility pump acts to decrease oceanic carbon uptake by only about 10 ppm and 4 ppm in the LL and high K_v models, respectively (compare the biological and full models in Table 5). The presence of ice has a very small impact of 3–8 ppm on the outcome of nutrient depletion experiments (Table 5). This is consistent with the small impact of ice on the surface to deep DIC gradient in both biological and soft-tissue models (Figure 2).

[42] In conclusion, given a full carbon cycle model undergoing surface nutrient depletion, most of the change in the total carbon pump and in the resulting atmospheric pCO_2 drawdown can be explained by variations in the soft-tissue pump. For simplicity, our analysis in the rest of the paper will focus exclusively on nutrient depletion simulations in the soft-tissue model without ice.

3.3. Theory: Atmospheric pCO_2 Sensitivity to Changes in the Soft-Tissue Pump

[43] Focusing on the soft-tissue pump, we propose a general theory on how atmospheric pCO_2 changes with preformed phosphate and the ocean carbon storage owing to this pump. We then apply our theory to understand atmospheric pCO_2 sensitivity to nutrient depletion.

[44] Nutrients are present in the ocean in two separate forms: as preformed and as remineralized nutrients. At the surface all nutrients are in the preformed form. If biology was perfectly efficient there would be no nutrients at the ocean surface, since all nutrients would be converted into organic matter. However, biology is not perfectly efficient and there are large quantities of so-called preformed, or biologically unutilized, nutrients left at the surface. Through photosynthesis, plants take preformed PO_4^{3-} and the associated CO_2 from the surface water and convert it into organic matter, which is respired (remineralized) below the euphotic layer into remineralized PO_4^{3-} and associated CO_2. Thus, in essence the soft-tissue pump acts to accumulate remineralized nutrients in the deep ocean while removing preformed nutrients from the ocean surface.

[45] In a soft-tissue model (where we disregard the calcium carbonate and solubility pumps), CO_2 is linked with remineralized PO_4^{3-} via a stoichiometric ratio $r_{C:P}$. The

total accumulation of dissolved inorganic carbon in the ocean due to the remineralization process can then be defined as the soft-tissue Ocean Carbon Storage (OCS_{soft}):

$$OCS_{soft} = r_{C:P} \cdot \overline{PO_{4\,remin.}} \cdot V_{oc} = r_{C:P} \cdot \left(\overline{PO_4^{3-}} - \overline{PO_{4\,pref}}\right) \cdot V_{oc}, \quad (2)$$

where V_{oc} is the ocean volume and an overline denotes global mean. OCS_{soft} is a measure of the soft-tissue pump strength. The stronger the soft-tissue pump, the more net accumulation of remineralized nutrients in the ocean and the stronger OCS_{soft} is.

[46] At every point in the ocean, DIC can be written as

$$DIC = DIC_{eq} + DIC_{diseq} + r_{C:P} \cdot PO_{4\,remin},$$

where the three terms are the components of DIC in equilibrium with the atmosphere, the component due to the air-sea CO_2 disequilibrium, and the net contribution from remineralization. DIC_{eq} and DIC_{diseq} are representative of the surface DIC values at the location (or locations) where this particular water parcel originated before it got subducted to the deep.

[47] For a soft-tissue only model, the total amount of inorganic carbon in the atmosphere-ocean system can therefore be written as

$$TC_{atm\,oc} = M_a \cdot pCO_{2\,a} + V_{oc} \cdot \overline{DIC_{eq}} + OCS_{soft} + V_{oc} \cdot \overline{DIC_{diseq}}, \quad (3)$$

where M_a is the mass of the atmosphere; and an overbar denotes global mean. The equilibrium (saturated) and the disequilibrium components of the carbon budget are $V_{oc} \cdot \overline{DIC_{eq}}$ and $V_{oc} \cdot \overline{DIC_{diseq}}$, respectively. $\overline{DIC_{eq}}$ is the globally averaged surface equilibrium DIC. For theoretical purposes we will assume that gas exchange is infinitely fast, such that CO_2 is in equilibrium with the atmosphere, surface DIC is exactly given by DIC_{eq} and there is no disequilibrium component $\overline{DIC_{diseq}} = 0$.

[48] For a given model we can perturb the system by changing the soft-tissue pump via nutrient depletion or via changes in oceanic circulation or mixing. Assuming that the total amount of inorganic carbon is kept constant we can write

$$\delta TC_{atm\,oc} = M_a \cdot \delta pCO_{2a} + V_{oc} \cdot \delta\overline{DIC_{eq}} + \delta OCS_{soft} = 0. \quad (4)$$

[49] The challenge is to find an analytical relationship between pCO_{2a} and OCS_{soft}. Making use of the average Revelle buffer factor at the ocean surface

$$R = \frac{\delta \ln pCO_{2\,a}}{\delta \ln DIC_{eq}} \simeq \frac{\delta pCO_{2\,a}}{\delta\overline{DIC_{eq}}} \cdot \frac{\overline{DIC_{eq}}}{pCO_{2\,a}},$$

we can derive

$$\frac{\delta pCO_{2a}}{\delta OCS_{soft}} = -\frac{pCO_{2a}}{Ma \cdot pCO_{2a} + V_{oc} \cdot \overline{DIC_{eq}}/R}. \quad (5)$$

[50] This equation was first analyzed by *Ito and Follows* [2005] who proposed that for small changes in atmospheric pCO_2 the right hand side of the equation is approximately constant. Defining

$$\gamma = 1 + V_{oc} \cdot \overline{DIC_{eq}}/(R \cdot M_a \cdot pCO_{2\,a})$$

and making the approximation

$$\gamma = \text{constant} \quad (6)$$

the solution to (5) is simply

$$pCO_{2a} = c_2 - \frac{OCS_{soft}}{M_a \cdot \gamma}, \quad (7)$$

where c_2 is a constant of integration.

[51] Below we show that such a linear approximation is insufficient to explain the sensitivity of atmospheric pCO_2 to changes in OCS_{soft} and we propose a more realistic solution to the differential equation (5).

[52] A first step in solving equation (5) is to rewrite $\overline{DIC_{eq}}/R$ as a function of pCO_{2a}. We note empirically from our model results that $\overline{DIC_{eq}}/R$ and pCO_{2a} are linearly related for a given alkalinity, T and S (Figure 3). For the alkalinity and pH values of the current ocean, the carbonate system acts as a buffer and ensures that an increase in gaseous CO_2 results in an increase in HCO_3^- and a decrease in CO_3^{2-}. We can show that to a first approximation $\overline{DIC_{eq}}/R$ is given by CO_3^{2-} (Figure 3) and is therefore a decreasing function of atmospheric pCO_2.

[53] We can therefore write to a good approximation,

$$V_{oc} \cdot \overline{DIC_{eq}}/R = a_1 - b \cdot pCO_{2\,a}, \quad (8)$$

where both a_1 and b are required by the buffer chemistry to be positive. We note that assumption (8) is fundamentally different from the assumption of *Ito and Follows* [2005] (equation (6)). We empirically determine from our simulations a_1 = 4089 PgC and b = 3.18 PgC/ppm, and we note that these parameters might change if alkalinity, T and S change.

[54] We now combine our approximation (8) with equation (5) and deduce

$$a_2 \cdot \frac{\partial pCO_{2a}}{\partial OCS_{soft}} \cdot pCO_{2a} + a_1 \cdot \frac{\partial pCO_{2a}}{\partial OCS_{soft}} + pCO_{2a} = 0,$$

where $a_2 = M_a - b$. We introduce the notation $pCO_{2a}' = \partial pCO_{2a}/\partial OCS_{soft}$ such that:

$$a_2 \cdot pCO_{2a}' \cdot pCO_{2a} + a_1 \cdot pCO_{2a}' + pCO_{2a} = 0. \quad (9)$$

[55] We now solve this equation for pCO_{2a} as a function of OCS_{soft}.

3.3.1. A Particular Solution

[56] In a previous paper [*Marinov et al.*, 2008] we proposed using the "conservation of buffered carbon" assumption of *Goodwin et al.* [2007]. Defining

$$C_{buffered} = M_a \cdot pCO_{2a} + V_{oc} \cdot \overline{DIC_{eq}}/R,$$

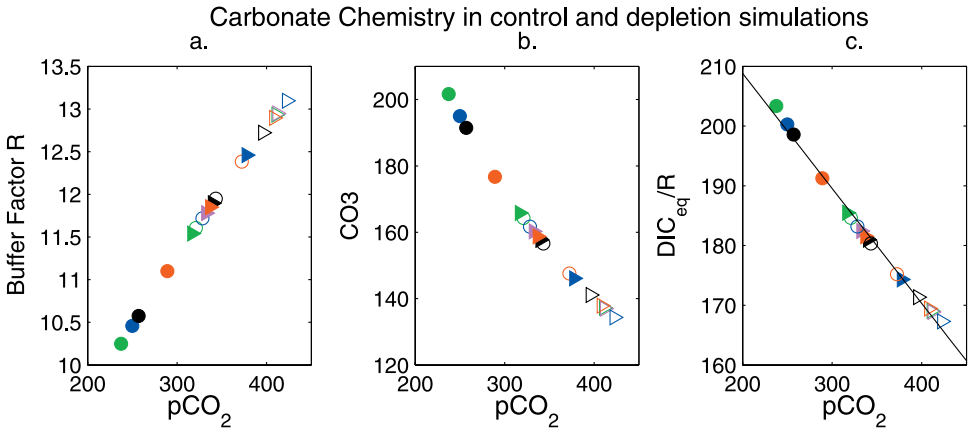

Figure 3. (a) Globally averaged Revelle or buffer factor R. (b) Globally averaged surface carbonate CO_3^{2-} (μmol/kg) and (c) globally averaged $\overline{DIC_{eq}}/R$ (PgC/a) plotted against atmospheric pCO_2 (ppm). Model results from both control (open symbols) and Southern Ocean depletion simulations (filled symbols) in fast gas exchange models. Symbols described in Figure 5 caption. Higher Southern Ocean ventilation models (triangles) have less carbonate and smaller DIC_{eq}/R compared to low-ventilation models (circles). Figure 3c is the basis for the linear approximation equation (8) and subsequent theoretical derivations.

where R is the Revelle or buffer factor and $\overline{DIC_{eq}}$ the globally averaged surface equilibrium DIC, the approximation

$$C_{buffered} \simeq \text{constant}, \tag{10}$$

holds reasonably well in our models. This approximation can be rewritten as

$$V_{oc} \cdot \overline{DIC_{eq}}/R = C_{buffered} - M_a \cdot pCO_{2a},$$

which compared to equation (8) gives $a_1 = C_{buffered}$, $b = M_a$, and $a_2 = M_a - b = 0$. Our differential equation (9) then becomes

$$a_1 \cdot pCO'_{2a} + pCO_{2a} = 0.$$

[57] In other words, applying Goodwin's approximation (10) is equivalent to setting $a_2 = 0$ in equation (9). The solution of this interesting particular case is an exponential,

$$pCO_{2a} = c \cdot e^{-\frac{OCS_{soft}}{a_1}} = c \cdot e^{-\frac{OCS_{soft}}{C_{buffered}}}, \tag{11}$$

where c is a constant of integration. For small deviations in pCO_{2a} from a reference state, a Taylor series expansion of (11) gives

$$\begin{aligned} pCO_{2\,a} &\simeq c_2 - \frac{pCO_{2\,a\,ref}}{C_{buffered}} \cdot OCS_{soft} \\ &= c_2 - \frac{pCO_{2\,a\,ref}}{C_{buffered}} \cdot r_{C:P} V_{oc} \cdot \left(\overline{PO_{4\,pref}} - \overline{PO_4}\right), \end{aligned}$$

which turns out to be identical with equation (7). Thus, the linear solution of *Ito and Follows* [2005] is an approximation to our exponential solution (11).

[58] We next show that relaxing Goodwin's approximation (i.e., allowing for nonzero a_2 values) leads to more complete solutions to our differential equation (9).

3.3.2. General Solution

[59] We now look for a solution to the nonlinear differential equation (9) when a_1 and a_2 are not zero. By treating the nonlinear term as a small perturbation we can deduce a general analytic solution to our differential equation. We show in Appendix B that our function pCO_{2a} can be written as a sum of exponentials of increasing power,

$$\begin{aligned} pCO_{2a} = c \cdot e^{-\frac{OCS_{soft}}{a_1}} &+ \frac{|a_2|}{a_1} \cdot c^2 \cdot e^{\frac{-2 \cdot OCS_{soft}}{a_1}} \\ &+ \frac{3}{2}\frac{|a_2|^2}{a_1^2} \cdot c^3 \cdot e^{\frac{-3 \cdot OCS_{soft}}{a_1}} + \ldots, \end{aligned} \tag{12}$$

where $a_1 = 4089$ PgC and $a_2 = -1.0602$ PgC/ppm are empirically derived.

[60] We note that each of these terms is positive and gradually smaller. Therefore, the first-order approximation to our function,

$$pCO_{2a\,(o)} = c \cdot e^{-\frac{OCS_{soft}}{a_1}}, \tag{13}$$

is a lower limit to our full solution (12). We note that $pCO_{2a(o)}$ is exactly the particular solution (11) to our differential equation when Goodwin's approximation (10) is assumed and therefore $a_2 = 0$. This proves that Goodwin's assumption, based on a particular linearization of the carbon chemistry, is meaningful, allowing a zeroth-order approximation of the general solution and providing a tight lower limit to our solution. This is demonstrated visually in Figure 4 (compare green and blue lines).

[61] How close the general solution is to the sum of the first exponential terms will depend on the relative values of the coefficients a_1 and a_2. For our particular system, Figure 4 demonstrates that the first two terms in the expansion (12) are almost indistinguishable from the numerical solution to our general equation and explain

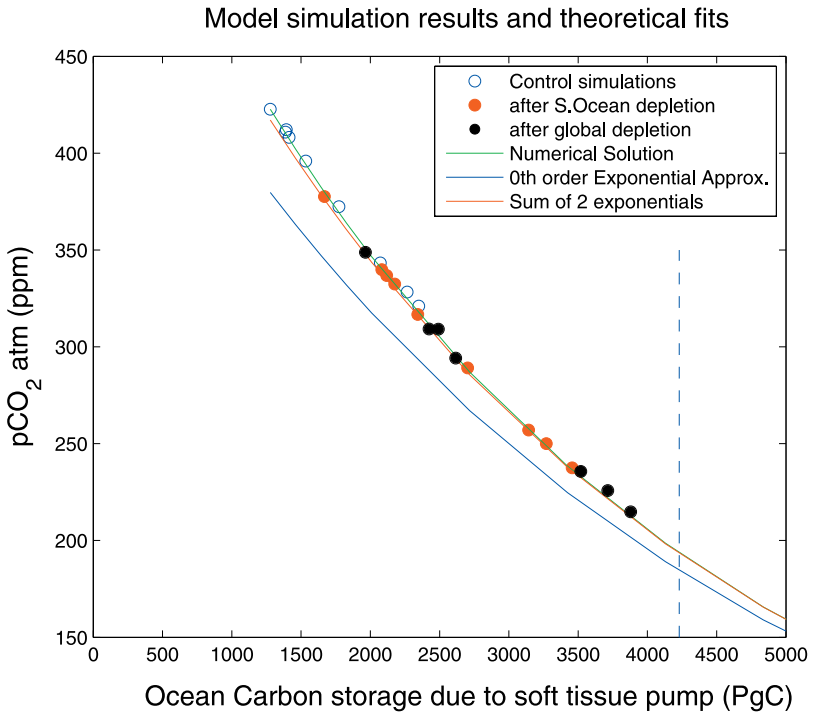

Figure 4. New theory predicts well the variation of atmospheric pCO_2 (ppm) with the ocean carbon storage due to the soft-tissue pump $OCS_{soft} = V_{oc} \cdot r_{C:P} \cdot (\overline{PO_4} - \overline{PO_{4pref}})$ (PgC). Fast gas exchange assumed. Shown are control (blue circles), Southern Ocean depletion (red), and global depletion simulations (black). Each set of simulations performed for eight of our soft-tissue models with different circulation regimes. Numerical Runge Kutta solution to the general differential equation (9) shown in green. The zeroth-order exponential approximation (equation (13), above in blue) is a lower limit and matches the full solution for OCS_{soft} very large. The sum of two exponentials (equation (16), above in red) closely predicts the numerical solution (in green) and agrees well with the model results (circles). The maximum OCS_{soft} that can be theoretically achieved in our models is 4230 PgC, the carbon equivalent of the total phosphorus inventory (vertical line).

remarkably well all our model results (Figure 4; compare red and green lines).

3.3.3. Sensitivity of pCO_{2a} With Respect to OCS_{soft}

[62] We proceed to study the derivatives of atmospheric pCO_2 with respect to OCS_{soft}. Rewriting equation (9) we get

$$pCO'_{2a} = -\frac{pCO_{2a}}{a_2 \cdot pCO_{2a} + a_1}. \tag{14}$$

On the other hand, taking the derivative of (9), combining it with (14) and rearranging terms yields

$$pCO''_{2a} = \frac{a_1 \cdot pCO_{2a}}{(a_2 \cdot pCO_{2a} + a_1)^3}. \tag{15}$$

We are only interested in positive values of pCO_{2a}. Since a_2 is negative, it is evident that $a_2 \cdot pCO_{2a} + a_1$ is positive for $pCO_{2a} < -a_1/a_2$, i.e., for all atmospheric pCO_2 values less than about 4000 ppm. The carbon buffering reactions at realistic pH and alkalinity require that a_1 calculated from equation (8) is positive. This implies via (14) and (15) that $pCO'_{2a} < 0$ and $pCO''_{2a} > 0$. Thus pCO_{2a} is a decreasing function of OCS_{soft} and pCO'_{2a} is an increasing function of OCS_{soft}. Consequently, the sensitivity of pCO_{2a} to changes in biology, defined as $S = -pCO_{2a}{}'$, is a decreasing function of OCS_{soft}.

[63] In summary, atmospheric pCO_{2a} and its sensitivity to biology are positive decreasing functions of OCS_{soft} approximately given by

$$pCO_{2a} \simeq c \cdot e^{-\frac{OCS_{soft}}{a_1}} + \frac{|a_2|}{a_1} \cdot c^2 \cdot e^{\frac{-2 \cdot OCS_{soft}}{a_1}} \tag{16}$$

$$S = -\frac{\partial pCO_{2a}}{\partial OCS_{soft}} \simeq \frac{c}{a_1} \cdot e^{-\frac{OCS_{soft}}{a_1}} + \frac{2|a_2|}{a_1^2} \cdot c^2 \cdot e^{\frac{-2 \cdot OCS_{soft}}{a_1}}. \tag{17}$$

The larger OCS_{soft}, the smaller the sensitivity, i.e., the less sensitive atmospheric pCO_2 becomes to further changes in OCS_{soft}. This interesting consequence will be discussed in section 3.4.

3.4. What is the Role of Mixing and Southern Ocean Winds in the Outcome of Nutrient Depletion Experiments?

[64] Changes in oceanic mixing and Southern Ocean westerlies can have a sizable impact on the amount of

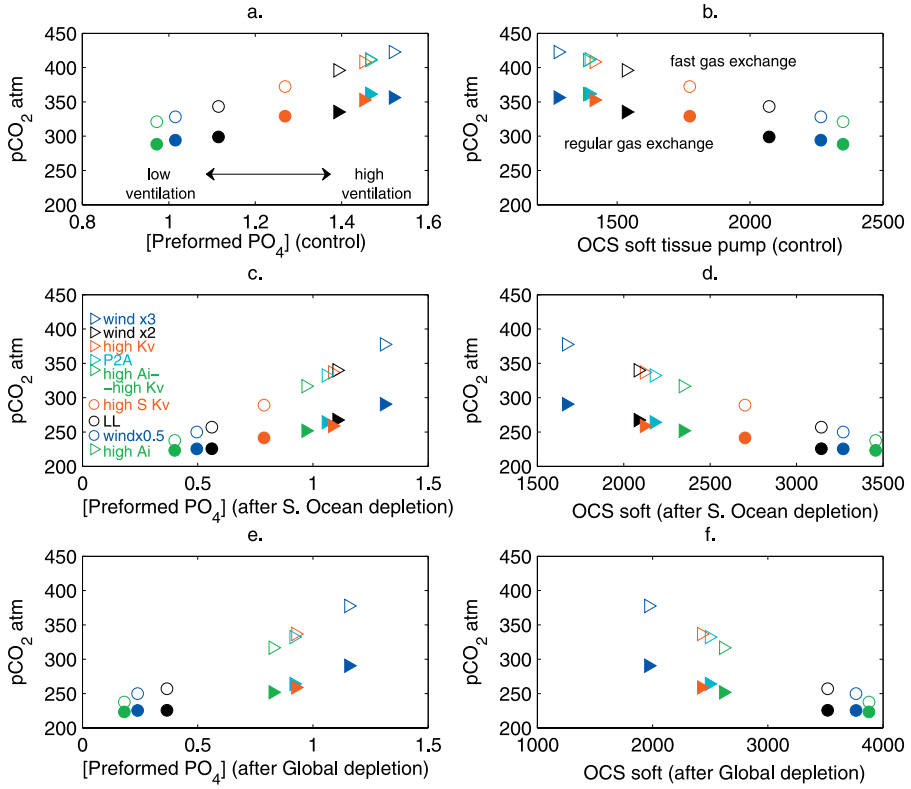

Figure 5. Atmospheric pCO_2 (ppm) versus globally averaged preformed PO_4 (μmol/kg) and versus OCS_{soft} (PgC) (a, b) in the control simulations, (c, d) after Southern Ocean depletion, and (e, f) after global depletion of surface nutrients. The ocean carbon storage due to the soft-tissue pump calculated as $OCS_{soft} = V_{oc} \cdot r_{C:P} \cdot (\overline{PO_4} - \overline{PO_{4pref}})$. Results shown for both fast gas exchange simulations (open triangles and circles) and regular gas exchange simulations (filled triangles and circles). Shown are the LL (black circle), high A_i (green circle), high south K_v (red circle), windx0.5 (blue circle), P2A (light blue triangle), windx2 (black triangle), windx3 (blue triangle), high K_v (red triangle), and high K_v-high A_i (green triangle) models. Circles denote lower Southern Ocean ventilation models; triangles denote higher-ventilation models.

carbon stored in the ocean, the preformed PO_4^{3-} inventory and atmospheric pCO_2 [*Marinov et al.*, 2008]. The present section compares the outcome of Southern Ocean and global nutrient depletion simulations in a suite of soft-tissue models in which diapycnal mixing, isopycnal mixing, and Southern Ocean winds are varied. We apply the theory developed in section 3.3 to understand the atmospheric pCO_2 sensitivity to changes in surface nutrients.

[65] As a model tracer, preformed PO_4^{3-} is set equal to PO_4^{3-} at the ocean surface and is thereafter allowed to advect and diffuse without additional biological sources or sinks. Since both preformed and total phosphate are model tracers, we can calculate the ocean carbon storage due to the soft-tissue pump OCS_{soft} directly from equation (2).

[66] Let us first consider results from the control simulations shown in Figures 5a and 5b. We broadly divided our models into low Southern Ocean ventilation models (LL, windx2, high A_i) or high Southern Ocean ventilation models (high K_v, P2A, high A_i-high K_v, windx2, windx3), depending on the strength of deep water ventilation. Increasing vertical mixing or Southern Ocean winds increases deep ocean ventilation and Southern Ocean convection (as indicated by less negative deep ocean $\Delta^{14}C$ values in Figure 1g and Table 6) while at the same time it increases Southern Ocean surface preformed nutrients. Both higher surface PO_4^{3-} south of 30°S and stronger deep ocean ventilation via the Southern Ocean contribute to higher $PO_{4\ pref}$ in the deep ocean. The correlation between deep ocean ventilation and the oceanic inventory of $PO_{4\ pref}$ is indicated by a remarkable $\Delta^{14}C$ - $\overline{PO_{4pref}}$ correlation (Figure 1g).

[67] High-ventilation models partition more of their carbon in the atmospheric pool and less in the oceanic pool compared to the low-ventilation models. Control simulations in high-ventilation models are therefore characterized by high deep ocean preformed phosphate, low remineralized phosphate, low OCS_{soft} and higher atmospheric pCO_2 compared to the low-ventilation models (compare triangles and circles in Figures 5a and 5b).

[68] How do models with different circulations respond to surface nutrient depletion?

[69] Surface nutrient depletion results in an increase in the export of organic matter out of the euphotic layer and a decrease in surface preformed PO_4^{3-} (Figures 6e and 6f and auxiliary material Figure S1[1]). Following Southern Ocean nutrient depletion, the negative surface signal of preformed

[1]Auxiliary materials are available in the HTML. doi:10.1029/2007JC004598.

Table 6. Results From Southern Ocean Depletion Experiments in Nine Soft-Tissue Pump Models With Fast Gas Exchange and Regular Gas Exchange[a]

	Model								
	High A_i	windx0.5	std (LL)	High south K_v	windx2	P2A	HH	High K_v	windx3
$\Delta^{14}C$	−254.7	−231.7	−196.7	−170.6	-	−151.8	−127.0	−112.2	−101.9
				Fast Gas Exchange					
pCO_{2a} Ctrl	321.0	328.3	343.3	372.4	395.9	412.0	410.9	408.2	422.7
OCS_{soft} Ctrl	2350	2266	2072	1773	1534	1394	1388	1413	1278
$\overline{PO_{4pref}}$ Ctrl	0.97	1.02	1.12	1.27	1.39	1.46	1.46	1.45	1.52
CO_3 Ctrl (%)	0.077	0.075	0.073	0.068	0.065	0.063	0.063	0.063	0.061
ΔpCO_{2a}	−83.4	−78.3	−86.3	−83.7	−56.0	−79.7	−94.1	−71.4	−45.1
ΔOCS_{soft}	1107	1004	1071	929	549	782	955	705	390
ΔPO_{4pref}	−0.57	−0.52	−0.55	−0.48	−0.29	−0.41	−0.50	−0.37	−0.21
S	0.075	0.078	0.081	0.090	0.102	0.102	0.099	0.101	0.116
				Regular Gas Exchange					
pCO_{2a} Ctrl	288.3	294.2	299.0	329.2	335.3	361.7	361.2	352.8	356.2
ΔpCO_{2a}	−65.1	−68.8	−73.3	−87.7	−68.0	−97.6	−109.3	−93.8	−65.7
S	0.059	0.068	0.068	0.094	0.124	0.125	0.114	0.133	0.168

[a]Models are arranged in order of increasing deep ocean ventilation as measured by their mean ocean $\Delta^{14}C$ at 1500 m. Shown are atmospheric pCO_2 (ppm), OCS_{soft} (PgC) and mean preformed PO_4 (μmol/kg) in the control simulations, as well as their respective changes with nutrient depletion. The percent of surface ocean DIC in the form of CO_3^{2-} shown for the control simulations. Also shown is the sensitivity of atmospheric pCO_2 to nutrient depletion, $S = -\Delta pCO_2/\Delta OCS_{soft}$. S is strongest for high-ventilation models characterized in the control simulations by high OCS_{soft} and low preformed PO_4.

PO_4^{3-} is either propagated via the AABW to the deep ocean, or advected northward via the AAIW and SAMW pathways (Figure 7, middle). The net result of depletion in all models is a decrease in the net deep preformed nutrients and in the global preformed nutrient inventory.

[70] Figures 5c and 5d and Figures 5e and 5f summarize results from Southern Ocean depletion and global surface nutrient depletion, respectively, in nine different circulation models. Since globally averaged total PO_4^{3-} is a constant in all our model experiments, a decrease in globally averaged

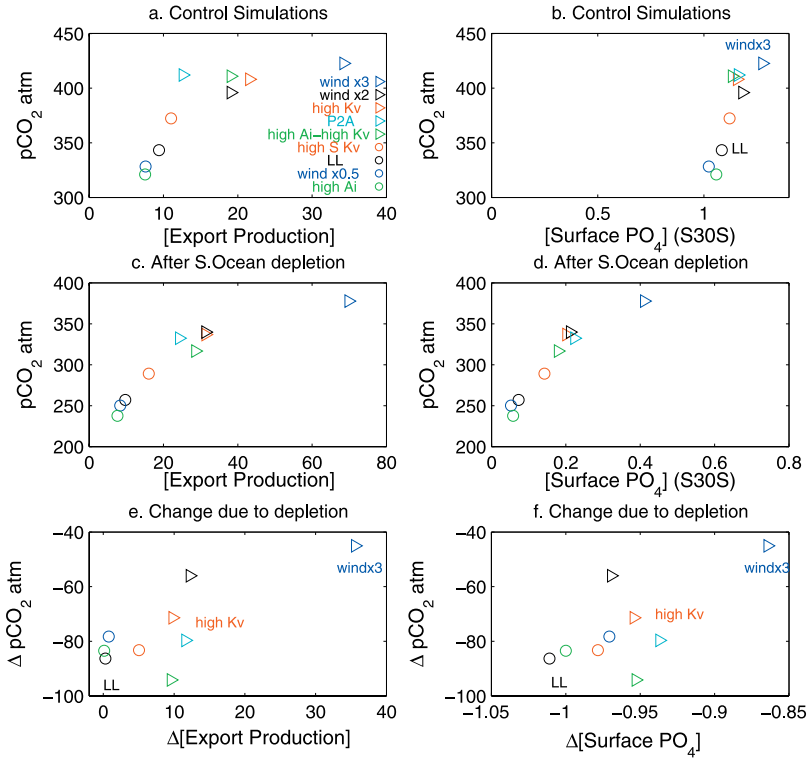

Figure 6. Atmospheric pCO_2 (ppm) versus globally averaged export production (PgC/a) and globally averaged surface PO_4 south of 30°S (μmol/kg) (a, b) in the control simulations, and (c, d) after Southern Ocean nutrient depletion. (e, f) The difference between the Southern Ocean nutrient depletion and control simulations. Fast gas exchange assumed. Symbols as in Figure 5. Export production and surface PO_4 (or equivalently surface preformed PO_4) are not good predictors for pCO_{2a}.

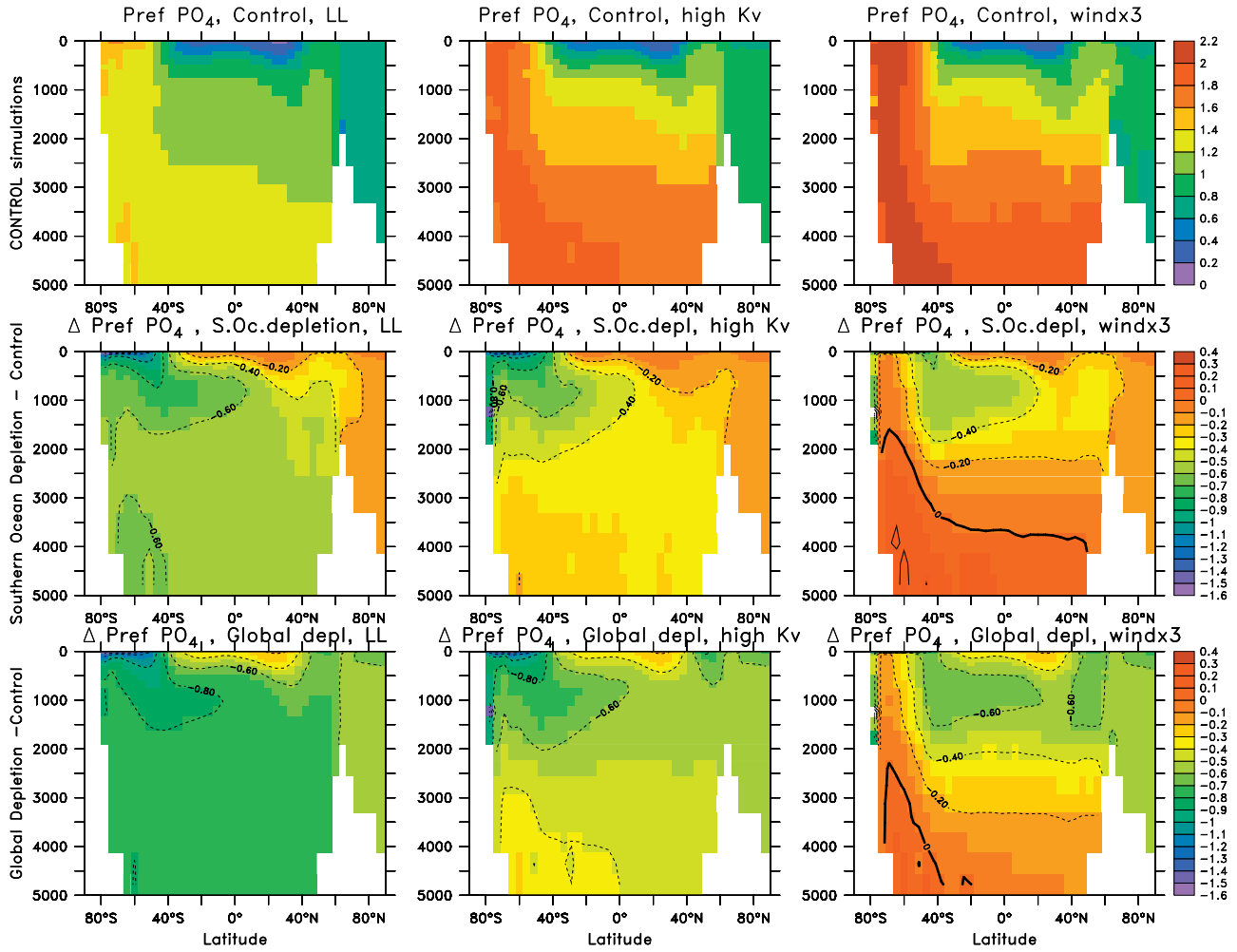

Figure 7. (top) Preformed PO_4 in the control GCMs. The change in preformed PO_4 due to (middle) Southern Ocean nutrient depletion and (bottom) global nutrient depletion. Global zonal averages shown in all cases for the standard (LL), high K_v, and windx3 GCMs. Units are μmol/kg. Depletion decreases the net deep preformed PO_4 more in the low-ventilation LL model compared to the high-ventilation models (high K_v, windx3). Some local elevation of preformed nutrients with depletion in the windx3 model reflects the complex regional interconnection of circulation and biology.

preformed PO_4^{3-} with depletion is equivalent to an increase in globally averaged remineralized PO_4^{3-} and an increase in the remineralized carbon inventory, OCS_{soft} (equation (2)). In a closed system in which total inorganic carbon in the system is constant the increase in OCS_{soft} results in lower atmospheric pCO_2. Figure 5 shows that this relationship is robust in all simulations performed.

[71] Figure 4 explores how well our new theory explains the model results. Each model simulation is represented by a point on this plot. Shown are results from control simulations and Southern Ocean simulations in all nine circulation models, as well as results from global nutrient depletion simulations in six of our circulation models. Large-scale nutrient depletion increases strongly the ocean carbon storage, decreasing significantly pCO_{2a}. Our theoretical solution (equation (16)) provides a remarkably good fit for the entire broad range of OCS_{soft} values, for a large spectrum of models with different circulations and different levels of surface nutrient depletion.

[72] Can we understand how the atmospheric pCO_2 drawdown depends on model circulation? Southern Ocean surface nutrients are set by a subtle balance between export production, which tends to decrease nutrients, and the resupply of nutrients from below via advection and convection. Under nutrient depletion conditions, increasing export production acts to decrease preformed phosphate. In the high-ventilation models stronger upwelling of nutrients to the surface counteracts some of this decrease. We note that this is possible because of a rather long (30 day) timescale used for restoring nutrients to zero, which allows nutrients to partly adjust to the oceanic circulation. Thus, while surface PO_{4pref} south of 30°S decreases in all models, the decrease is on average smaller in high-ventilation models compared to low-ventilation models (Figure 6f and auxiliary material) This has implications for the deep preformed phosphate balance.

[73] Following Southern Ocean nutrient depletion, Southern Ocean surface preformed phosphate decreases and the

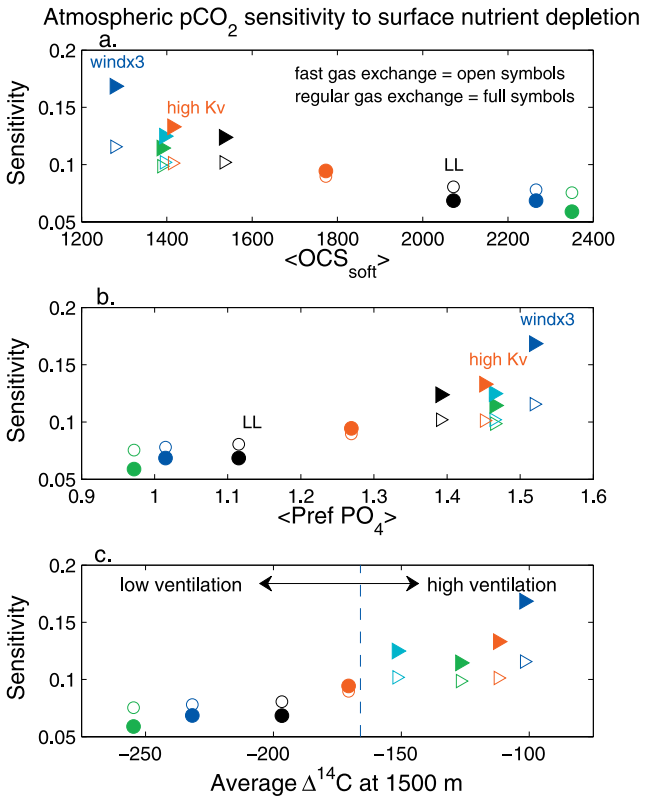

Figure 8. Sensitivity of atmospheric pCO_2 to Southern Ocean nutrient depletion plotted against (a) ocean carbon storage $OCS_{soft} = r_{C:P} \cdot (\overline{PO_4} - \overline{PO_{4pref}})$ before depletion (i.e., in the control simulation), (b) globally averaged preformed PO_4^{3-} before depletion, and (c) globally averaged $\Delta^{14}C$ at 1500 m depth. Sensitivity defined as $-\Delta\ pCO_{2a}/\Delta OCS_{soft}$. Fast gas exchange (open symbols) and regular gas exchange simulations (filled symbols) shown for our model suite. Symbols as in Figure 5. High-ventilation models (triangles) have higher sensitivity than lower ventilation models (circles). Regular gas exchange enhances this effect. The vertical line in Figure 8c shows the observed $\Delta\ ^{14}C$ at 1500 m from GLODAP.

negative preformed signal is propagated to the deep ocean via AABW. Because the surface decrease in preformed PO_4^{3-} is much smaller in the high-ventilation models, the resulting deep preformed nutrient decrease is smaller in these models compared to the low-ventilation models, as illustrated in Figure 7. Less decrease in deep preformed PO_4^{3-} following nutrient depletion signals more accumulation of remineralized PO_4^{3-} and carbon in the deep and less atmospheric pCO_2 drawdown in the high-ventilation models compared to the low-ventilation models (Table 6).

[74] In our global depletion simulations nutrients are restored to zero everywhere at the ocean surface. While high-latitude surface nutrients drop significantly, they are not completely depleted (auxiliary material Figure S1). Therefore, true global depletion was not achieved in any of our models. Assuming global depletion was possible, the carbon storage in the ocean would be at its maximum when

$$OCS_{soft}^{max} = r_{C:P} \cdot \overline{PO_4} \cdot V_{oc} = 4230\ \text{PgC}.$$

This is the maximum OCS_{soft} for all models regardless of circulation, and is therefore a natural limit in Figure 4.

3.4.1. Sensitivity of Atmospheric pCO_2 to Nutrient Depletion

[75] We argue here that the most interesting quantity which needs to be compared across all models is the sensitivity of atmospheric pCO_2 to nutrient depletion, defined as

$$S = -\frac{\Delta pCO_{2a}}{\Delta OCS_{soft}} = \frac{1}{r_{C:P}} \cdot \frac{\Delta pCO_{2a}}{\Delta \overline{PO_{4pref}}},$$

where Δ stands for the changes observed with depletion.

[76] Figure 8 shows how S varies across our models. Given identical total air-sea carbon inventories, high-ventilation models partition more of their carbon in the atmosphere and less in the ocean relative to low ventilation models. Because of their higher atmospheric carbon content, high-ventilation models have more surface aqueous CO_2 and bicarbonate (HCO_3^-) and, because of buffer chemistry, less surface carbonate compared to the low-ventilation models (Figure 3). Carbonate buffers changes in surface CO_2. Lower concentration of surface carbonate implies less capacity to buffer changes in surface CO_2 following nutrient depletion. This explains why high-ventilation models are more sensitive to nutrient depletion than lower ventilation models: S(high ventilation) >S(low ventilation).

[77] The dependence of sensitivity on OCS_{soft} can also be illustrated graphically with a thought experiment. Let us refer to Figure 9, which is an idealized curve representing the solution to our general differential equation (9). The sensitivity of atmospheric pCO_2 to changes in ocean carbon storage, S, is just the absolute value of the slope at a given point. If, for example, the preformed inventory and therefore OCS_{soft} changed by the same amount in a low- and a high-ventilation model, in which model would atmospheric pCO_2 decrease more? Assuming

$$\Delta\overline{PO_{4pref}}(\text{low vent}) = \Delta\overline{PO_{4pref}}(\text{high vent}) \text{ and}$$
$$\Delta OCS_{soft}(\text{low vent}) = \Delta OCS_{soft}(\text{high vent}),$$

Figure 9 geometrically implies that the high-ventilation model is more sensitive to changes in biology,

$$|\Delta pCO_2(\text{high vent})| > |\Delta pCO_2(\text{low vent})| \text{ and}$$
$$S(\text{high ventilation}) > S(\text{low ventilation}),$$

which is exactly what we notice in our simulations.

[78] Figure 8 confirms that the sensitivity of atmospheric pCO_2 to nutrient depletion decreases with OCS_{soft} and increase with the preformed PO_4^{3-} inventory, in agreement with equation (17).

[79] Mathematically, this interesting result is a consequence of the nonlinearity of the relationship between pCO_{2a} and OCS_{soft} implied by equation (16). Carbonate chemistry requires that $a_1 > 0$, which ensures that pCO_2 and S are decreasing exponential functions of OCS_{soft}. If instead pCO_{2a} and OCS_{soft} were linearly related as in (7), a given increase in OCS_{soft} would result in the same decrease in pCO_{2a} regardless of the initial value of OCS_{soft}. This would

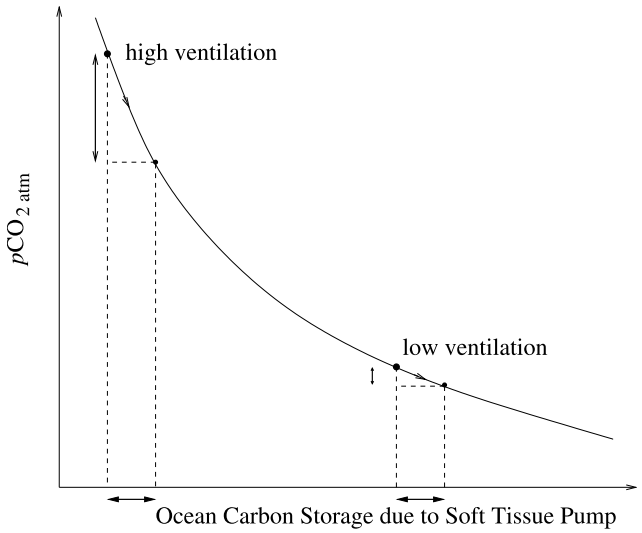

Figure 9. Idealized plot of atmospheric pCO_2 decrease with the soft-tissue ocean carbon storage, $OCS_{soft} = V_{oc} \cdot r_{C:P} \cdot (\overline{PO_4} - \overline{PO_{4pref}})$. Since the relationship is nonlinear, sensitivity $S = -\Delta pCO_2/\Delta OCS_{soft}$ is larger for smaller OCS_{soft}. Therefore a high-ventilation model is more sensitive than a low-ventilation model to changes in OCS_{soft}. If the relationship was linear, S would be identical for all values of OCS_{soft}, i.e., for all models. This is clearly not the case.

incorrectly imply that all our models are equally efficient at drawing down atmospheric pCO_2; that is, S is identical in all the models, in disagreement with Figure 8.

3.5. What is the Role of Gas Exchange in Nutrient Depletion Experiments?

[80] Sections 3.3 and 3.4 assumed that CO_2 exchange at the ocean surface is infinitely fast, such that surface CO_2 was in equilibrium with the atmosphere. In reality, CO_2 at the ocean surface needs about nine months to equilibrate with the atmosphere. The slow CO_2 exchange with the atmosphere in the real ocean introduces departures from the theoretical relationship between OCS_{soft} and atmospheric pCO_2 discussed in sections 3.3 and 3.4. Surface CO_2 disequilibrium is set by a subtle interplay between circulation, gas exchange and biological restoring. We compare the outcome of nutrient depletion simulations in fast gas exchange scenarios with no surface CO_2 disequilibrium and realistic, regular gas exchange scenarios.

[81] Figure 10 shows that the response of atmospheric pCO_2 to a slower gas exchange is opposite in sign between high-ventilation models and low-ventilation models (compare full and open symbols). Slower gas exchange makes nutrient depletion less efficient in low-ventilation models but more efficient in high-ventilation models. How can we understand this behavior?

[82] In the high-ventilation models (P2A, high K_v, windx2, windx3) a slow air-sea CO_2 exchange relative to

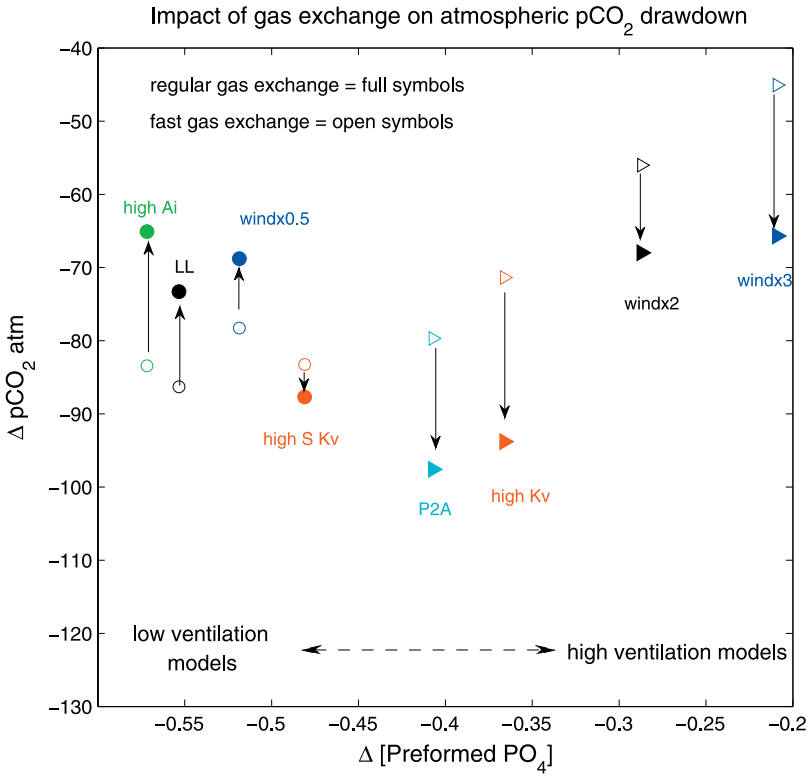

Figure 10. Impact of gas exchange on the outcome of surface nutrient depletion. Decrease in atmospheric pCO_2 (ppm) with depletion shown against the decrease in globally averaged preformed PO_4 (μmol/kg). Results of Southern Ocean depletion shown in both fast gas exchange models (open symbols) and slower, regular gas exchange models (filled symbols). Slower gas exchange makes depletion more efficient in high-ventilation models, while it makes depletion less efficient in low-ventilation models.

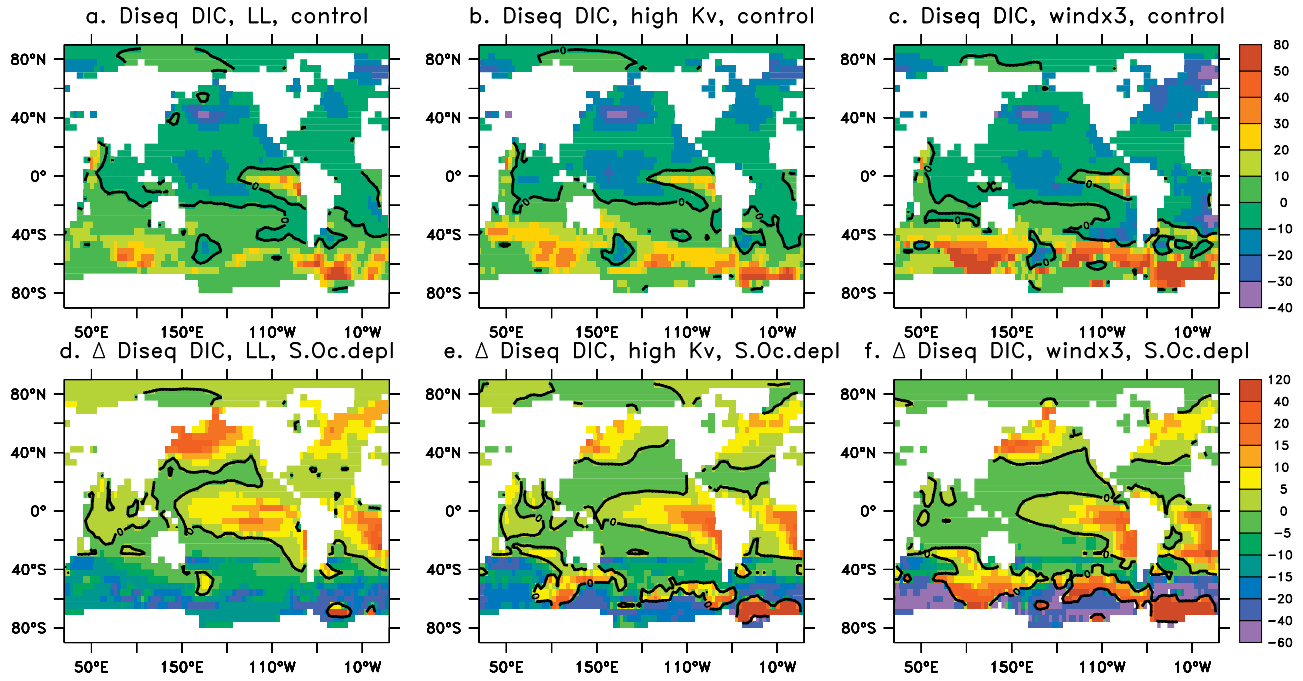

Figure 11. August surface disequilibrium DIC in the LL, high K_v, windx3 soft-tissue models with regular gas exchange. (top) Control simulations. (bottom) Change due to Southern Ocean depletion. Units are μmol/kg. Disequilibrium DIC calculated according to equation (18). Positive values indicate oversaturation with respect to the atmosphere. Depletion causes mostly Southern Ocean undersaturation in the LL model, and mostly Southern Ocean oversaturation in the windx3 model.

the ocean circulation and biology ensures that most of the CO_2 upwelled in the Southern Ocean is advected and taken up by biology before it has a chance to escape back to the atmosphere. Slow air-sea CO_2 exchange in the Southern Ocean upwelling areas acts to keep more carbon in the ocean and increase the efficiency of surface nutrient depletion. For our most realistic P2A model, atmospheric pCO_2 drawdown following nutrient depletion is 97.6 ppm in the regular gas exchange scenario compared to 79.7 ppm in the fast gas exchange scenario.

[83] We can understand more thoroughly this behavior by analyzing the distribution of disequilibrium DIC, which is set by the CO_2 supersaturation or undersaturation with respect to the atmosphere at the ocean surface and behaves like any conserved tracer in the ocean interior. For all points in the ocean, we calculate

$$\mathrm{DIC}_{diseq} = \mathrm{DIC} - \mathrm{DIC}_{eq} - R_{C:P} \cdot \left(\mathrm{PO}_4^{3-} - \mathrm{PO}_{4pref}\right), \qquad (18)$$

where the terms on the right-hand side are the total DIC, equilibrium DIC and the soft-tissue component of DIC, respectively. DIC, PO_4^{3-} and PO_{4pref} are model outputs, while DIC_{eq} is calculated from the standard carbonate system given values for atmospheric pCO_2, Alk, T and S. For a given soft-tissue model simulation there is a unique value of DIC_{eq} characterizing all surface points (since Alk, T and S are kept constant in the gas exchange calculation). We note, however, that DIC_{eq} changes value after nutrient depletion because the corresponding atmospheric pCO_2 value changes.

[84] The surface disequilibrium DIC during August for three of our models with regular gas exchange is shown in Figure 11. Positive DIC_{diseq} signals supersaturation. Most oceanic convection and deep water formation happens during the Southern Hemisphere winter; disequilibrium surface values at this time will affect the CO_2 concentration in waters feeding the ocean interior and will have most impact on the ocean carbon budget and atmospheric pCO_2.

[85] Let us first analyze our control simulations. For each of our models, surface waters are slightly undersaturated in CO_2 in tropical regions where biology is efficient. Conversely, Southern Ocean surface waters are supersaturated in the control simulations (Figures 11a–11c). This makes sense. Biology is generally unable to take up all of the CO_2 upwelled in the Southern Ocean, and inorganic carbon therefore accumulates at the ocean surface as positive DIC_{diseq}. In models with stronger Southern Ocean upwelling (P2A, high K_v, windx2, windx3), biology is less efficient relative to upwelling of nutrients from below the surface and surface CO_2 supersaturation is necessarily higher than in the LL model. The surface signal is reflected in the deep ocean distribution of disequilibrium DIC (Figures 12a–12c). Low-latitude thermocline waters are undersaturated. The deep ocean is oversaturated in CO_2, reflecting the Southern Ocean surface supersaturation. Stronger AABW results in more deep ocean oversaturation.

[86] Depleting Southern Ocean surface nutrients changes the degree of surface CO_2 equilibration via two mechanisms which work against each other: (1) a biological mechanism and (2) a circulation mechanism. (1) A more efficient biology can take up some of the additional CO_2 from the

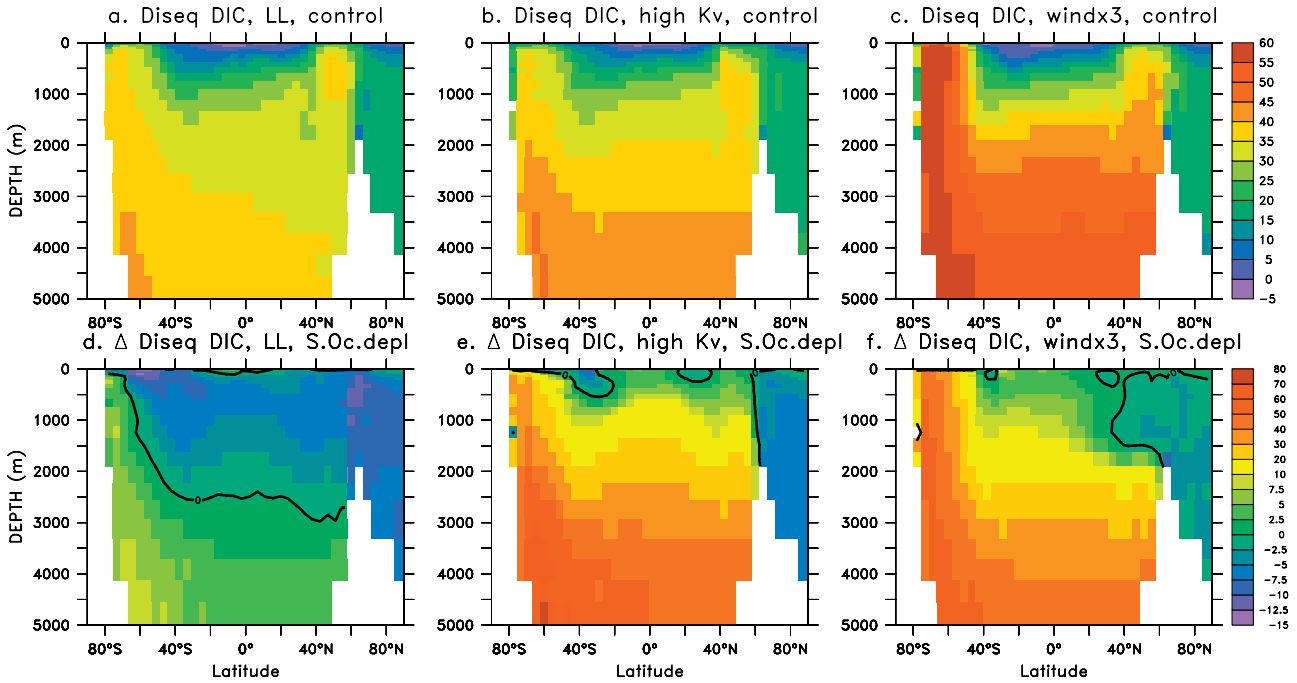

Figure 12. Vertical profiles of disequilibrium DIC (μmol/kg) in the LL, high K_v, windx3 soft-tissue models with regular gas exchange. Annual averages. (top) Control simulations. (bottom) Change due to Southern Ocean depletion. Depletion causes mostly undersaturation in the LL model, and oversaturation in the high K_v and windx3 models.

Southern Ocean surface, acting to decrease surface disequilibrium DIC (i.e., decrease the surface CO_2 oversaturation) when gas exchange is slow. (2) Nutrient depletion increases the amount of remineralized CO_2 stored in the deep and intermediate ocean. Some of this additional CO_2 is upwelled to the surface in the Southern Ocean upwelling and convective regions. Upwelling therefore tends to increase the CO_2 oversaturation at the surface and the surface disequilibrium DIC.

[87] In a low-ventilation model such as LL, Southern Ocean upwelling is rather weak and little additional CO_2 is upwelled to the surface. Additionally, surface circulation is slow such that CO_2 rich water is exposed long enough to the atmosphere to be close to equilibrium even when gas exchange is slow. Mechanism 2 above is therefore rather inefficient and mechanism 1 dominates. In most areas, a more efficient biology following nutrient depletion decreases surface DIC disequilibrium in the Southern Ocean (Figure 11d). This undersaturation signal (expressed as negative DIC_{diseq}) is advected by the strong AAIW and AMW toward the North Atlantic and fills much of the ocean at intermediate depths (Figure 12d). The result is a decrease in the global inventory of DIC_{diseq} with depletion, which drives a decrease in the total inorganic carbon stored in the ocean. In other words, the presence of surface disequilibrium makes the ocean store less carbon than it would if CO_2 was perfectly equilibrated with the atmosphere. Atmospheric pCO_2 drawdown following nutrient depletion is smaller in the LL, high A_i and windx0.5 regular gas exchange models compared to the corresponding fast gas exchange models (Figure 10). In low-ventilation models, slow gas exchange makes nutrient depletion less efficient.

[88] By contrast, in the high-ventilation models (P2A, high K_v, windx2, windx3), Southern Ocean upwelling is strong and mechanism 2 dominates. Additionally, surface circulation is fast such that the upwelled CO_2 rich waters do not have time to equilibrate with the atmosphere before sinking again. This results in increased surface CO_2 supersaturation and thus an increase in surface disequilibrium DIC in the Weddell Sea and Southern Ocean upwelling locations (Figures 11e and 11f). This supersaturation signal is downwelled in deep water formation regions and results in an increase in the global inventory of DIC_{diseq} with depletion, as shown by Figures 12e and 12f and Table 6. Thus, in models with fast Southern Ocean circulation, the presence of surface disequilibrium helps the ocean store more CO_2 than it would if CO_2 was in equilibrium with the atmosphere. In these models, the impact of disequilibrium is significant: a 10–20 ppm increase in atmospheric pCO_2 drawdown.

[89] In conclusion, slower gas exchange has opposite effects on the outcome of nutrient depletion experiments in the low-ventilation versus high-ventilation models. The same separation between the low- and high-ventilation models behavior emerges in both Southern Ocean nutrient depletion and global depletion simulations.

4. Discussion

[90] In this paper we propose a new theory for how atmospheric pCO_2 varies with the preformed phosphate inventory and the oceanic carbon storage due to the soft-tissue pump, OCS_{soft}. This theory is an improvement over two previous approximations [*Marinov et al.*, 2008; *Ito and*

Follows, 2005] and posits that atmospheric pCO_2 can be written as a sum of exponential functions of OCS_{soft}. While the preformed nutrient inventory and OCS_{soft} are robust metrics for atmospheric pCO_2, export production and surface nutrients on their own are not (Figure 6).

[91] The Southern Ocean drives most of the biological pump in the world ocean because of the effective communication between the surface and deep ocean and the large concentration of surface preformed (i.e., biologically unutilized) nutrients here. As a consequence, Southern Ocean depletion strengthens the global biological pump and draws down atmospheric pCO_2 significantly: by 63.5 ppm and by 74 ppm for the LL and high K_v models with fully represented carbon pumps, respectively. Southern Ocean nutrient depletion is much more effective than depleting nutrients in the North Atlantic, North Pacific or tropical regions (Table 4). The soft-tissue pump governs the atmospheric CO_2 response to surface nutrient depletion in realistic ocean GCMs. Despite their considerable contributions to the total carbon pump, we show that the carbonate and the solubility pumps have a small impact on the outcome of surface nutrient depletion (Table 5 and Figure 2).

[92] The response of atmospheric pCO_2 to large-scale surface nutrient depletion in our suite of soft-tissue ocean GCMs depends strongly on deep ocean ventilation, as summarized by Table 6 and Figures 9 and 10.

[93] Assuming surface ocean CO_2 equilibrates with the atmosphere instantaneously, we can predict atmospheric pCO_2 and the sensitivity of atmospheric pCO_2 to nutrient change from the preformed nutrient inventory of the ocean. The theoretical solution (16) is shown to hold robustly both before and after surface nutrient depletion. Knowledge of the oceanic inventory of preformed PO_4^{3-} in a model indicates how sensitive this model is to nutrient forcing (equation (17)). A large inventory of preformed PO_4^{3-} (small OCS_{soft}) indicates high sensitivity to high-latitude nutrient forcing. This agrees with *Toggweiler et al.* [2003] who intuited that ocean models with a weak biological pump (i.e., smaller soft-tissue ocean carbon storage) should be more efficient at removing atmospheric pCO_2 in response to nutrient depletion than models with a stronger biological pump.

[94] Increasing vertical mixing or Southern Ocean winds increases deep ocean ventilation via AABW and Southern Ocean convection. This increases the relative contribution of the Southern Ocean preformed nutrients to the deep preformed nutrient inventory. High-ventilation models therefore have higher preformed nutrient inventory and lower ocean carbon storage due to the soft-tissue pump (or OCS_{soft}) compared to low-ventilation models. This implies, from the previous paragraph, that high-ventilation models should be more sensitive to changes in the soft-tissue pump. Our simulations confirm that increasing deep ocean ventilation via the Southern Ocean circulation makes atmospheric pCO_2 more sensitive to Southern Ocean nutrient depletion (Figure 10). Our work contradicts the findings of *Archer et al.* [2000] who suggested that vertical diffusion acts to break the monopoly of high latitudes in determining atmospheric pCO_2.

[95] The warm interglacial climates partitioned more of their carbon in the atmosphere and less in the ocean compared to the glacial climates. It increasingly appears that this is due to a stronger deep ocean ventilation during interglacials [e.g., *Marchitto*, 2007; *Toggweiler*, 2008; *Toggweiler and Russell*, 2008]. Assuming that the total ocean-atmosphere carbon between glacials and interglacials did not vary much, this would imply, according to our results, that atmospheric pCO_2 is more sensitive to changes in nutrients (such as those occurring via iron fertilization) during interglacials than during glacials.

[96] Our results might also have interesting consequences for the future climate. For example, if Southern Ocean circulation will intensify with global warming (following either an increase or poleward shift in Southern Ocean westerlies), atmospheric pCO_2 might become ever more sensitive to changes in Southern Ocean surface biology. One important caveat is that our theory assumes a closed system in which the total amount of inorganic carbon is kept constant. Studies of the soft-tissue pump in an open system which allows for increasing anthropogenic carbon are needed to generalize our present results.

[97] The theoretical relationship between pCO_{2a} and preformed PO_4 (or OCS_{soft}) derived in section 3.3 is based on a simplification of the carbon system. While the $CaCO_3$ and solubility pump were shown to have a small impact on the outcome of our Southern Ocean nutrient depletion experiments, they are nonetheless important terms which we need to understand for climatic purposes. Future theoretical derivations should attempt to also incorporate the $CaCO_3$ pump, solubility pump and disequilibrium components.

[98] In the real ocean, surface CO_2 exchange with the atmosphere is slow. The degree of CO_2 disequilibrium impacts carbon storage in the deep ocean and the atmospheric pCO_2 sensitivity to surface nutrient depletion. The impact of CO_2 disequilibrium is considerable and depends on oceanic circulation. In models with strong AABW and Southern Ocean upwelling the slow air-sea CO_2 exchange in the Southern Ocean upwelling areas acts to keep more carbon in the ocean and increase the efficiency of nutrient depletion. CO_2 disequilibrium therefore acts to make atmospheric pCO_2 in high-ventilation models even more sensitive to high-latitude nutrient forcing. The opposite is true in slow ventilation models, where surface CO_2 disequilibrium makes atmospheric pCO_2 less sensitive to surface nutrient depletion (Figure 10).

[99] Previous studies of the natural carbon pumps [*Archer et al.*, 2000; *Broecker et al.*, 1999] have suggested that various GCMs have different sensitivities to high-latitude forcing, as measured by their abiotic pCO_2 or by their HBEI index. Our study shows clearly that one must be extremely careful when comparing different models and when designing comparison indices. Differences in diapycnal or isopycnal mixing or boundary conditions, can result in significant differences in preformed nutrients and atmospheric pCO_2 sensitivity to high-latitude forcing. Additionally, the amount of surface CO_2 disequilibrium (which also impacts atmospheric pCO_2) is very sensitive to whether one is in a high Southern Ocean ventilation regime or in a low Southern Ocean ventilation regime. This reinforces the importance of getting the correct circulation in our models.

[100] We note again that in order for our theoretical consideration to hold, the amount of inorganic carbon in

the air-sea system (i.e., the total CO_2 in the atmosphere plus the total DIC in the ocean) has to be the same for all models and kept constant at all times. Nutrient depletion might result in a different atmospheric pCO_2 drawdown in models with different total DIC. We suggest that future studies of the natural carbon pumps and model comparison studies take into account this very important constraint.

[101] In conclusion, we have shown that the oceanic soft-tissue pump and atmospheric pCO_2 in GCMs are very sensitive to changes in mixing, Southern Ocean winds or nutrient forcing in high latitudes. Our proposed theory can help us understand the response of atmospheric pCO_2 to circulation changes and surface nutrient depletion. Our findings support a strong role for the high latitudes and in particular for the Southern Ocean in the cycling of organic carbon.

Appendix A: Separating the Various Carbon Pumps in Our Models

[102] In order to separate the carbon pumps from each other in our models we consider three different scenarios: a full carbon pump scenario, a biology pump only scenario and a soft-tissue pump scenario, as explained below.

[103] 1. A first, full carbon pump scenario includes the biogeochemistry model detailed in section 3.2.1. In this setup, surface pCO_2 and the air-sea CO_2 exchange depend on seasonally and spatially varying T, S, DIC, and ALK at each surface grid point. For our rigid lid ocean model, we account for the diluting/concentrating effects of evaporation and precipitation through virtual fluxes of DIC and ALK.

[104] 2. In a second biology pump only scenario the ocean temperature and salinity are set constant everywhere at the surface and equal to 10°C and 34.7 psu, respectively, for the purpose of the CO_2 gas exchange calculation. This operation shuts off the solubility pump, such that the oceanic distribution of DIC does not depend any more on the surface T and S variability. Virtual fluxes of DIC and ALK (which are essentially abiotic) are switched off.

[105] 3. Finally, in our soft-tissue pump scenario we turn off the solubility and carbonate pumps by (1) setting surface ocean T and S constant in the CO_2 gas exchange calculations, and (2) by setting alkalinity constant and equal everywhere to the initializing value, ALK = 2370 umol/kg. The virtual fluxes of DIC and ALK are again switched off. This scenario was used by *Marinov et al.* [2006].

[106] *Marinov and Sarmiento* [2004] showed that we can linearly separate the soft-tissue, carbonate and solubility carbon pumps from a complex model by simplifying our model as described above. For example, the DIC contribution due to the solubility pump will simply be given by the difference in DIC from models run with full carbon pump versus biology only pump. Similarly, the DIC contribution due to the $CaCO_3$ pump is the DIC difference between the same physical model run in the biological pump only scenario and in the soft-tissue pump only scenario.

Appendix B: Theoretical Derivations

[107] Here we present an approximate analytic solution to the differential equation (9) by treating the nonlinear term as a perturbation. Using the notation $y = pCO_{2a}$, $x = OCS_{soft}$, $y' = \partial y/\partial x = \partial pCO_{2a}/\partial OCS_{soft}$, equation (9) becomes

$$a_2 \cdot y' y + a_1 \cdot y' + y = 0. \tag{B1}$$

We assume a_1 not zero, a_2 negative and we write $a_2 = -|a_2|$ for clarity.

[108] For realistically small values of y, the second term in (B1) dominates the first term. To the zeroth order $y(x) \simeq y_{(o)}$ and we can write

$$a_1 \cdot y'_{(o)} + y_{(o)} = 0$$

with the solution $y_{(o)}(x) = c \cdot e^{-\frac{x}{a_1}}$, where c is a constant of integration. To zero order y is a decreasing exponential of x.

[109] The nonlinear term in (B1) gives a small correction to this which we write as $y(x) \simeq y_{(o)}(x) + y_{(1)}(x)$. Plugging this expression into (B1) and keeping only $y'_{(o)} \cdot y_{(o)}$ and higher terms, we get

$$a_1 \cdot y'_{(1)} + y_{(1)} = |a_2| \cdot y'_{(o)} y_{(o)} = -\frac{|a_2|}{a_1} c^2 \cdot e^{\frac{-2x}{a_1}}$$

with solution

$$y_{(1)} = \frac{|a_2|}{a_1} \cdot c^2 \cdot e^{\frac{-2x}{a_1}}.$$

This procedure can be repeated to arbitrary order. For instance, to a second order, $y(x) \simeq y_{(o)}(x) + y_{(1)}(x) + y_{(2)}(x)$. We plug this expression again into (B1), keep only the linear terms in $y_{(1)}$ and arrive at an equation for $y_{(2)}$ which can be solved exactly:

$$y_{(2)} = \frac{3}{2} \frac{|a_2|^2}{a_1^2} \cdot c^3 \cdot e^{\frac{-3x}{a_1}}.$$

The general solution to equation (B1) therefore is $y(x) = y_{(o)}(x) + y_{(1)}(x) + y_{(2)}(x) + \ldots$ or

$$y = c \cdot e^{-\frac{x}{a_1}} + \frac{|a_2|}{a_1} \cdot c^2 \cdot e^{\frac{-2x}{a_1}} + \frac{3}{2} \frac{|a_2|^2}{a_1^2} \cdot c^3 \cdot e^{\frac{-3x}{a_1}} + \ldots.$$

We note that this procedure gives a valid approximation only in the regime in which the derivative y' is well behaved (i.e., continuous) and negative. This, as we discuss in section 3.3, requires that $a_2 \cdot y + a_1 > 0$, i.e., $y < a_1/|a_2|$. For a realistic choice of a_2 and a_1 such as $a_1 = 4089$ Pg C, $a_2 = -1.0602$ PgC/ppm, this implies y (i.e., atmospheric pCO_2) smaller than 3860 ppm, which is clearly within our regime of interest.

[120] More rigorously, one can solve recursively for higher-order coefficients using the infinite series methods for solving ODEs, i.e., by making the ansatz

$$y = \sum_{n=1}^{\infty} d_n \cdot e^{-nx/a_1}.$$

[121] **Acknowledgments.** While at MIT, I.M. was supported by the NOAA Postdoctoral Program in Climate and Global Change, administered by the University Corporation for Atmospheric Research. We are grateful to

R. Toggweiler for numerous discussions and for sharing his intuition on carbon cycle dynamics.

References

Archer, D. E., G. Eshel, A. Winguth, W. Broecker, R. Pierrehumbert, M. Tobis, and R. Jacob (2000), Atmospheric pCO_2 sensitivity to the biological pump in the ocean, *Global Biogeochem. Cycles*, *14*(4), 1219–1230.

Bacastow, R. B. (1996), The effect of temperature change of the warm surface waters of the oceans on atmospheric CO_2, *Global Biogeochem. Cycles*, *10*(2), 319–334.

Boyd, P. W., et al. (2007), Mesoscale iron enrichment experiments 1993–2005: Synthesis and future directions, *Science*, *315*(5812), 612–617.

Broecker, W., J. Lynch-Stieglitz, D. Archer, M. Hofmann, E. Maier-Reimer, O. Marchal, T. Stocker, and N. Gruber (1999), How strong is the Harvardton-Bear constraint?, *Global Biogeochem. Cycles*, *13*(4), 817–821.

Bryan, K., and L. J. Lewis (1979), A water mass model of the world ocean, *J. Geophys. Res.*, *84*(C5), 2503–2517.

Buesseler, K. O., J. E. Andrews, S. M. Pike, and M. A. Charette (2004), The effects of iron fertilization on carbon sequestration in the Southern Ocean, *Science*, *304*(5669), 414–417.

Dutkiewicz, S., M. J. Follows, and P. Parekh (2005), Interactions of the iron and phosphorus cycles: A three-dimensional model study, *Global Biogeochem. Cycles*, *19*(1), GB1021, doi:10.1029/2004GB002342.

Gent, P. R., and J. C. McWilliams (1990), Isopycnal mixing in Ocean circulation models, *J. Phys. Oceanogr.*, *20*(1), 150–155.

Gnanadesikan, A., R. D. Slater, N. Gruber, and J. L. Sarmiento (2002), Oceanic vertical exchange and new production: A comparison between models and observations, *Deep Sea Res., Part II*, *49*, 363–401.

Gnanadesikan, A., R. D. Slater, and B. L. Samuels (2003), Sensitivity of water mass transformation and heat transport to subgridscale mixing in coarse-resolution ocean models, *Geophys. Res. Lett.*, *30*(18), 1967, doi:10.1029/2003GL018036.

Gnanadesikan, A., J. P. Dunne, R. M. Key, K. Matsumoto, J. L. Sarmiento, R. D. Slater, and P. S. Swathi (2004), Oceanic ventilation and biogeochemical cycling: Understanding the physical mechanisms that produce realistic distributions of tracers and productivity, *Global Biogeochem. Cycles*, *18*(4), GB4010, doi:10.1029/2003GB002097.

Goodwin, P., R. G. Williams, M. J. Follows, and S. Dutkiewicz (2007), Ocean-atmosphere partitioning of anthropogenic carbon dioxide on centennial timescales, *Global Biogeochem. Cycles*, *21*(1), GB1014, doi:10.1029/2006GB002810.

Hellerman, S., and M. Rosenstein (1983), Normal monthly wind stress over the world ocean with error estimates, *J. Phys. Oceanogr.*, *13*, 1093–1104.

Ito, T., and M. J. Follows (2005), Preformed phosphate, soft tissue pump and atmospheric CO_2, *J. Mar. Res.*, *63*(4), 813–839, doi:10.1357/0022240054663231.

Knox, F., and M. B. McElroy (1984), Changes in atmospheric CO_2: Influence of the marine biota at high latitude, *J. Geophys. Res.*, *89*(D3), 4629–4637.

Louanchi, F., and R. G. Najjar (2000), A global climatology of phosphate, nitrate and silicate in the upper ocean: Spring-summer production and shallow remineralization, *Global Biogeochem. Cycles*, *14*(3), 957–977.

Marchitto, T. M. (2007), Marine radiocarbon evidence for the mechanism of deglacial atmospheric CO_2 rise, *Science*, *316*(5830), 1456–1459.

Marinov, I., and J. L. Sarmiento (2004), The role of the oceans in the global carbon cycle: An overview, in *Ocean Carbon Cycle and Climate*, edited by M. Follows and T. Oguz, pp. 251–295, Kluwer Acad., Norwell, Mass.

Marinov, I., A. Gnanadesikan, J. R. Toggweiler, and J. L. Sarmiento (2006), The Southern Ocean biogeochemical divide, *Nature*, 964–967, doi:10.1038/nature04883.

Marinov, I., et al. (2008), Impact of oceanic circulation on biological carbon storage in the ocean and atmospheric pCO_2, *Global Biogeochem. Cycles*, doi:10.1029/2007GB002958, in press.

Martin, J. H. (1990), Glacial-interglacial CO_2 change: The iron hypothesis, *Paleoceanography*, *5*(1), 1–13.

Matear, R. J., and B. Elliott (2004), Enhancement of oceanic uptake of anthropogenic CO_2 by macronutrient fertilization, *J. Geophys. Res.*, *109*, C04001, doi:10.1029/2000JC000321.

Najjar, R. G., et al. (2007), Impact of circulation on export production, dissolved organic matter, and dissolved oxygen in the ocean: Results from Phase II of the Ocean Carbon-cycle Model Intercomparison Project (OCMIP-2), *Global Biogeochem. Cycles*, *21*, GB3007, doi:10.1029/2006GB002857.

Pacanowski, R. C., and S. M. Griffies (1999), *The MOM3 Manual, Alpha Version*, 580 pp., Geophys. Fluid Dyn. Lab., NOAA, Princeton, N. J.

Petit, J. R., et al. (1999), Climate and atmospheric history of hte past 420,000 yars from the Vostok ice core, Antarctica, *Nature*, *399*, 429–436.

Sarmiento, J. L., and J. C. Orr (1991), Three-dimensional ocean model simulations of the impact of Southern Ocean nutrient depletion on atmospheric CO_2 and ocean chemistry, *Limnol. Oceanogr.*, *36*, 1928–1950.

Sarmiento, J. L., and J. R. Toggweiler (1984), A new model for the role of the oceans in determining atmospheric pCO_2, *Nature*, *308*, 620–624.

Siegenthaler, U., and T. H. Wenk (1984), Rapid atmospheric CO_2 variations and ocean circulation, *Nature*, *308*, 624–626.

Toggweiler, J. R. (2008), Origin of the 100,000-year timescale in Antarctic temperatures and atmospheric CO_2, *Paleoceanography*, *23*, PA2211, doi:10.1029/2006PA001405.

Toggweiler, J. R., and J. Russell (2008), Ocean circulation in a warming climate, *Nature*, *451*, 286–288.

Toggweiler, J. R., R. Murnane, S. Carson, A. Gnanadesikan, and J. L. Sarmiento (2003), Representation of the carbon cycle in box models and GCMs—Part 2. Organic pump, *Global Biogeochem. Cycles*, *17*(1), 1027, doi:10.1029/2001GB001841.

Volk, T., and M. I. Hoffert (1985), Ocean carbon pumps: Analysis of relative strengths and efficiencies in ocean driven atmospheric CO_2 changes, in *The Carbon Cycle and Atmospheric CO_2: Natural Variations Archaean to Present*, *Geophys. Monogr. Ser.*, vol. 32, edited by E. T. Sundquist and W. S. Broecker, pp. 99–110, AGU, Washington, D. C.

M. J. Follows, Department of Earth, Atmospheric and Planetary Sciences, Massachusetts Institute of Technology, 77 Massachusetts Avenue, EAPS Building 54, Cambridge, MA 02139, USA. (mick@ocean.mit.edu)

A. Gnanadesikan, Geophysical Fluid Dynamics Laboratory, P.O. Box 308, Princeton, NJ 08542, USA. (gnana@princeton.edu)

I. Marinov, Department of Marine Chemistry and Geochemistry, Woods Hole Oceanographic Institution, MS 25, 360 Woods Hole Road, Woods Hole, MA 02543, USA. (imarinov@whoi.edu)

J. Sarmiento and R. Slater, Atmospheric and Oceanic Sciences Program, Princeton University, Sayre Hall, Forestall Campus, P.O. Box CN710, Princeton, NJ 08544-0710, USA. (jls@princeton.edu; rdsalter@splash.princeton.edu)